nature ecology & evolution

Article

https://doi.org/10.1038/s41559-024-02485-7

Sugar assimilation underlying dietary evolution of Neotropical bats

Received: 6 July 2023

Accepted: 27 June 2024

Published online: 28 August 2024

Check for updates

Jasmin Camacho[1,4] ✉, Andrea Bernal-Rivera[1,2,4], Valentina Peña[1], Pedro Morales-Sosa[1], Sofia M. C. Robb[1], Jonathon Russell[1], Kexi Yi[1], Yongfu Wang[1], Dai Tsuchiya[1], Oscar E. Murillo-García[2] ✉ & Nicolas Rohner[1,3] ✉

Dietary specializations in animals lead to adaptations in morphology, anatomy and physiology. Neotropical bats, with their high taxonomic and trophic diversity, offer a unique perspective on diet-driven evolutionary adaptations. Here we assess the metabolic response to different dietary sugars among wild-caught bats. We found that insectivorous bats had a pronounced metabolic response to trehalose, whereas bats with nectar and fruit-based diets showed significantly higher blood glucose levels in response to glucose and sucrose, reaching levels over 750 mg dl^{-1}. The genomic analysis of 22 focal species and two outgroup species identified positive selection for the digestive enzyme trehalase in insect eaters, while sucrase–isomaltase showed selection in lineages with omnivorous and nectar diets. By examining anatomical and cellular features of the small intestine, we discovered that dietary sugar proportion strongly impacted numerous digestive traits, providing valuable insight into the physiological implications of molecular adaptations. Using hybridization chain reaction (HCR) RNA fluorescence in situ hybridization, we observed unusually high expression in the glucose transporter gene *Slc2a2* in nectar bats, while fruit bats increased levels of *Slc5a1* and *Slc2a5*. Overall, this study highlights the intricate interplay between molecular, morphological and physiological aspects of diet evolution, offering new insights into the mechanisms of dietary diversification and sugar assimilation in mammals.

Organisms adapt to their environments to improve their chances of survival and reproductive success. Throughout animal evolution, diet is a major environmental input that influences adaptations in nutrient acquisition, such as feeding morphology and behaviour[1–8]. Changes in metabolism underlie these diet-related evolutionary variations, affecting the ability of cells and tissues to sense and respond to altered nutrient availability. This ability is crucial for maintaining energy homoeostasis and overall health[9–13].

Glucose homoeostasis is a tightly regulated biochemical pathway that maintains circulating glucose levels within a narrow physiological range for cellular function and organismal energy. Blood glucose levels fluctuate throughout the day, are easily measured and relate to lifestyle and diet[14]. This pathway is expected to have a critical role in metabolic adaptations[15]. However, wildlife studies investigating these adaptations are scarce and include few taxa[16–20]. Existing research is primarily focused on accessible lab populations of wild animals[21–25] or restricted within the context of metabolic disorders[26,27].

Natural systems exhibiting a wide diversity of diets, such as in bats, provide a unique opportunity to investigate diet-related evolutionary changes. Bats have diversified from an insect-heavy ancestral diet to

[1]Stowers Institute for Medical Research, Kansas City, MO, USA. [2]Grupo de Investigación en Ecología Animal, Departamento de Biología, Universidad del Valle, Cali, Colombia. [3]Department of Molecular and Integrative Physiology, University of Kansas Medical Center, Kansas City, KS, USA. [4]These authors contributed equally: Jasmin Camacho, Andrea Bernal-Rivera. ✉e-mail: jcamacho@stowers.org; oscar.murillo@correounivalle.edu.co; nro@stowers.org

nutritional sources including fruit, nectar, meat and fish, among others[28,29]. The dietary shifts among bats reflect the evolutionary changes across major clades of mammals[30,31], such as herbivores, omnivores and carnivores (that is, orders Artiodactyla, Primates and Carnivora). Therefore, investigating their adaptive radiation is expected to provide new perspectives on the diversification of metabolic traits and emphasize the molecular basis of these adaptations.

In this study, we explore the metabolic adaptations involved in dietary changes over evolutionary time. We observe adaptation to the glucose homoeostasis pathway across 29 bat species with different diets, using three dietary sugars—trehalose (found in insects' hemolymph), sucrose and glucose (both found in fruits and nectar). We demonstrate that the metabolic phenotype is mediated by four different adaptations to digestive morphology, including intestinal length, exposed villi and enterocyte and microvilli number. We have discovered genetic traits linked to maximal extraction of glucose energy from nutritional resources associated with diet. These include positive selection on genes encoding the digestive enzymes TREH, trehalase (*Treh*), and SI, sucrase–isomaltase (*SI*), as well as glucose transporters GLUTs, solute carrier family 2 members 1–5 (*Slc2a1–5*). We investigated the effects of these amino acid substitutions on protein function through structural comparisons. Additionally, we observed a change in the expression of genes encoding transporters SLC2A2 (*Slc2a2* gene), SCL2A5 (*Slc2a5* gene) and SLC5A1 (*Slc5a1* gene) in response to an acute glucose meal within enterocytes along the brush border of the small intestine. The emerging picture illustrates the sophisticated adaptability of absorptive villi, highlighting the evolution of traits and mechanisms that enable species to utilize a broader range of nutrient resources compared with those found ancestrally. Overall, this study advances our understanding of how metabolic evolution contributes to species diversification.

Results and discussion

In vivo physiology

Bats provide a unique perspective on metabolic adaptations due to their high energetic demands and diverse diets. They have specialized from an ancestor with an insect-heavy diet to fruit, nectar, meat, blood and other food sources[28]. To assess metabolic adaptations related to dietary diversification, we focused on the glucose homoeostasis pathway, which regulates glucose energy between meals and is crucial for health and survival. We performed in vivo oral glucose tolerance tests on 199 wild-caught bats across 29 species (Extended Data Table 1) to assess their ability to process three dietary sugars[32,33]: trehalose (formed by two glucose molecules), sucrose (formed by glucose and fructose) and glucose. Wild-caught bats were fasted for 10–12 h, and blood glucose levels were measured before and after consuming a single sugar meal (5.4 g kg^{-1}(ref. 22)). Measurements were taken at 10, 30 and 60 min post-ingestion, revealing distinct patterns in the rise and fall of blood glucose levels between dietary guilds (Fig. 1a). To better quantify physiological responses, we classified them into four assimilation patterns, 'fast', 'medium', 'slow' and 'limited' (Fig. 1b), on the basis of the speed and extent of assimilation (see 'General patterns of sugar assimilation curves' section in Methods).

In insectivorous and omnivorous bats, we observed trehalose assimilation with blood glucose levels reaching up to 160 mg $dl^{-1}$with a 'slow' tolerance curve indicating glucose absorption continuing until 60 min. In contrast, bats with nectar and fruit diets exhibited a 'limited' ability to assimilate trehalose, showing blood glucose levels remaining within a narrow range and only rising to 60 mg dl^{-1}. These findings align with existing evidence that the trehalase gene (*Treh*) is non-functional in non-insectivorous mammals, including bats, and functional in omnivores[34,35], such as *Carollia* and *Phyllostomus*. Interestingly, vampire bats showed a slight rise and fall in blood glucose levels following trehalose consumption, reaching levels of 90 mg dl^{-1}. We propose that the minor elevation in blood glucose levels in non-insectivorous bats may be linked to gut microbiome activity[36,37], as trace amounts of trehalase were found in their gut[34].

When tested for sucrose, insect-feeding bats showed a gradual increase in blood glucose levels 30 min post-ingestion, except for *Myotis*, which showed a rapid rise to 200 mg dl^{-1} within 10 min, followed by a decline to 140 mg dl^{-1} at 60 min, indicating a 'medium' sucrose assimilation. This suggests that *Myotis* might be capable of sucrose digestion more efficiently than trehalose despite its classification as an insect feeder. As expected, vampire bats showed 'limited' sucrose assimilation, maintaining blood glucose levels below 96 mg dl^{-1} throughout the experiment. Among omnivores, *Carollia* levels peaked at 10 min (200 mg dl^{-1}) and gradually declined, whereas *Phyllostomus* had a lower peak at 10 min (100 mg dl^{-1}) and slowly decreased. These patterns reflect the varying degrees of omnivory, where *Carollia* mainly feed on piper fruits and some insects, while *Phyllostomus* consume insects, fruits, small vertebrates, flowers, nectar and pollen[38,39]. Fruit and nectar bats exhibited two major responses to sucrose: (1) 'fast' assimilation with a rapid rise in blood glucose (200 mg dl^{-1}) within 10 min and rapid decrease to basal levels after 60 min for *Artibeus, Dermanura* and *Choeroniscus* and (2) 'medium' assimilation with a slow increase, reaching a maximum after 30 min (300 mg dl^{-1}) for *Sturnira, Uroderma* and *Glossophaga*. These findings highlight notable variations in sucrose assimilation across and within dietary categories, suggesting diversified disaccharide assimilation mechanisms and potential seasonal impacts, meriting further study, especially for omnivorous bats.

When tested for glucose ingestion, we observed higher blood glucose levels across all bat species compared with trehalose and sucrose feedings, due to direct intestinal absorption of monosaccharides, unlike disaccharides, which require prior hydrolysis[30]. Bats with insect, meat and blood diets showed a gradual rise in blood glucose levels, staying under 300 mg dl^{-1}, except in *Pteronotus* (> 350 mg dl^{-1}) but still indicating a 'slow' assimilation pattern. Among omnivorous bats, *Carollia* peaked at 423 mg dl^{-1} at 10 min before rapidly declining by 60 min, while *Phyllostomus* reached a peak of 225 mg dl^{-1} at 30 min and declined by 60 min. Fruit bats, such as *Artibeus* and *Dermanura*, exhibited the most extreme rise and fall of blood glucose levels, reaching 600 mg dl^{-1} within 10 min and dropping to 100 mg dl^{-1} in some individuals after 60 min. This 'fast' assimilation curve is probably due to heightened insulin sensitivity in these species[40]. Other fruit bats showed high glucose levels within 30 min, with *Uroderma* reaching 476 mg dl^{-1} and *Sturnira* reaching 357 mg dl^{-1}, followed by a subsequent decrease. In nectarivores, we observed 'fast' assimilation curves, with *Glossophaga* and *Lonchophylla* reaching levels above the detection limit of 600 mg dl^{-1} (GlucoQuick G30a) at 10 min and *Choeroniscus* reaching 300 mg dl^{-1} at the 10-min timepoint, probably influenced by varying plant and nectar preferences[41,42]. In contrast, captive *Glossophaga soricina* individuals reached a peak of 360 mg dl^{-1} after 30 min when fed with a similar single dose and did not exceed 470 mg dl^{-1}, even with higher doses (9 g kg^{-1})[22]. Nectar bats from Glossophaginae and Lonchophyllinae subfamilies showed slower declines in blood glucose levels compared with fruit bats, aligning with studies suggesting glucose regulation through exercise rather than insulin response[22,43–46]. These findings highlight how sugar assimilation capability in Neotropical bats reflects their natural food preferences, raising questions about their ability to manage blood glucose fluctuations.

To evaluate the impact of evolutionary history on sugar assimilation, we employed Pagel's λ (ref. 47) to measure the phylogenetic signal for each assimilation pattern with the area under the glucose tolerance test curve as a proxy. We obtained λ values of 0.99 for sucrose assimilation ($P < 0.05$) (Extended Data Fig. 2). However, glucose and trehalose did not show a phylogenetic signal. These results suggest that phylogenetic relationships are probably playing an important role in determining sucrose assimilation but not in the monosaccharide or

https://doi.org/10.1038/s41559-024-02485-7

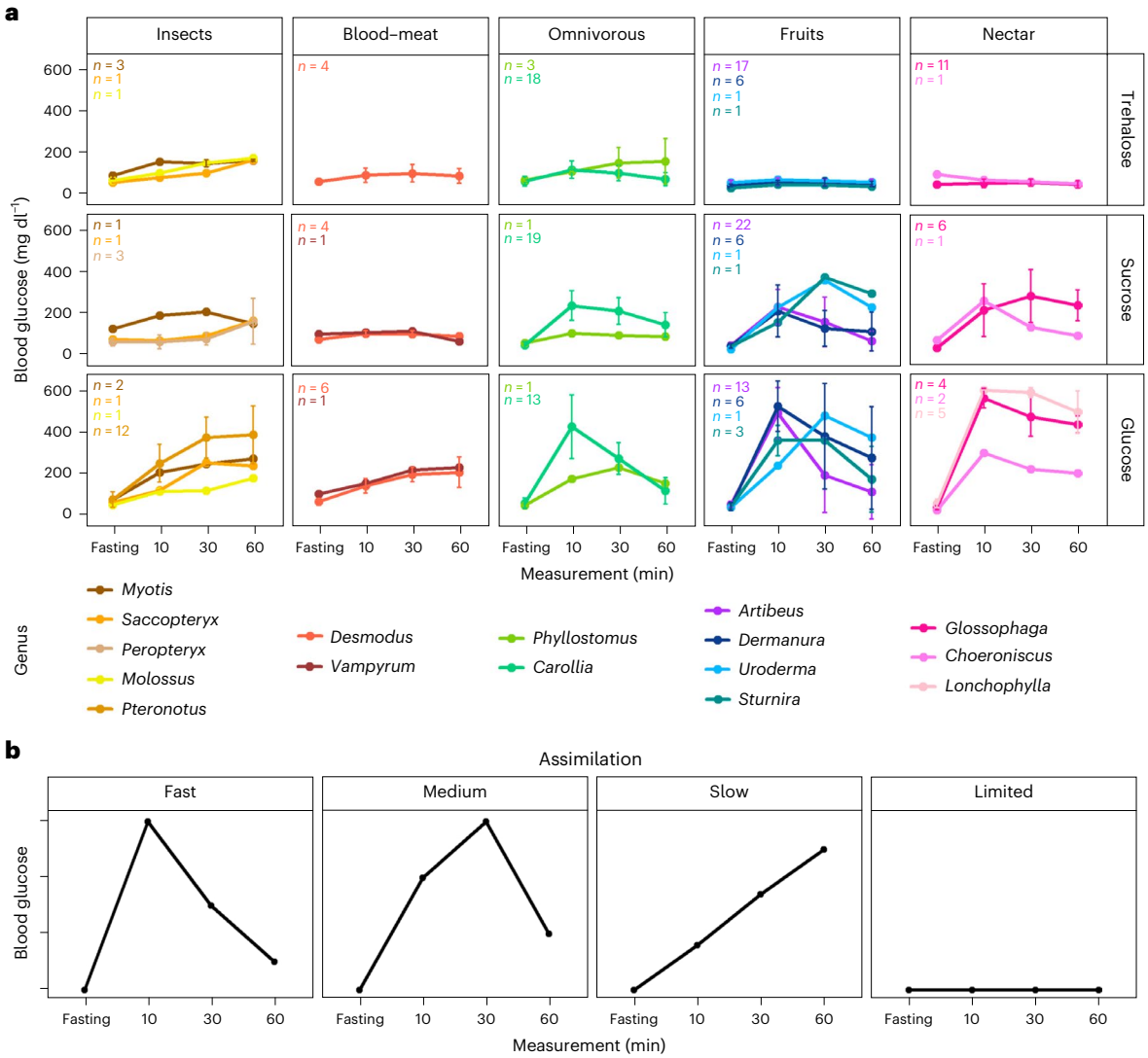

Fig. 1 | Glucose tolerance tests for three different dietary sugars. a, Average assimilation curves for trehalose, sucrose and glucose among Neotropical bats with different food preferences: insects, blood or meat, mixed (omnivorous), fruits and nectar. The sample size varied among genera from 1 to 52 individuals (Extended Data Table 1). The data are presented as mean values ± standard deviation for a sample size greater than three individuals. **b**, General curves to describe the temporal pattern of sugar assimilation.

trehalose assimilation, which is probably why we see most variation among species in response to glucose and the higher response to trehalose in insectivorous and omnivorous bats even when they are not closely related. This observation is consistent with a prior study that examined traits related to digestion and found that the gut surface area, body mass and digestion is not constrained by phylogeny[48]. Additionally, we fitted a Bayesian multi-level phylogenetic model to compare adaptations in glucose assimilation while controlling for phylogenetic relatedness. We found differences in the assimilation pattern of glucose, sucrose and trehalose between species with high- and low-sugar diets. However, the omnivorous bats, with the three sugars present in their diets, showed similar glucose and sucrose assimilation patterns to bats with rich glucose and sucrose diets (fruit and nectar bats) and similar trehalose assimilation patterns to bats with rich trehalose diets (insectivorous). This indicates a strong association between assimilation patterns and dietary preferences.

Molecular adaptations related to sugar assimilation

To identify molecular adaptations underlying the association between sugar assimilation and different diets, we tested genes involved in sugar digestion and transport for positive selection. We analysed genes encoding for the digestive enzyme TREH, trehalase (*Treh*), responsible for breaking down trehalose into glucose, and SI, sucrase–isomaltase (*SI*), which converts sucrose to glucose and fructose (Fig. 2a). We also examined genes encoding GLUTs, glucose transporters, involved in the absorption of these sugars from the intestinal lumen into the blood (Fig. 2a), including sodium/glucose co-transporter (*Slc5a1*), solute carrier family 2 member 2 (*Slc2a2*) and solute carrier family 2 member 5 (*Slc2a5*). Interestingly, while SLC2A5 functions as a transporter for fructose, it can also transport glucose[49,50]. Furthermore, transporters have crucial roles in directing circulating blood glucose into cells to fulfil tissue-specific energy demands[51] (Fig. 2b). These genes include *Slc2a1*, predominantly found in red blood cells and astrocytes[52]; *Slc2a2*, enriched in the intestine, liver, hypothalamus and pancreatic beta cells[53]; *Slc2a3*, mainly in neurons[54]; *Slc2a4*, expressed in insulin-sensitive tissues such as cardiac muscle, skeletal muscle and fat[55]; and *Slc2a5*, abundant in microglia, liver, kidney and testis[49].

We included 22 bats represented in our in vivo data (Fig. 2c), along with two outgroup species (Extended Data Table 3). Using adaptive branch-site random effects likelihood[56] (aBSREL) with HyPhy[57,58],

https://doi.org/10.1038/s41559-024-02485-7

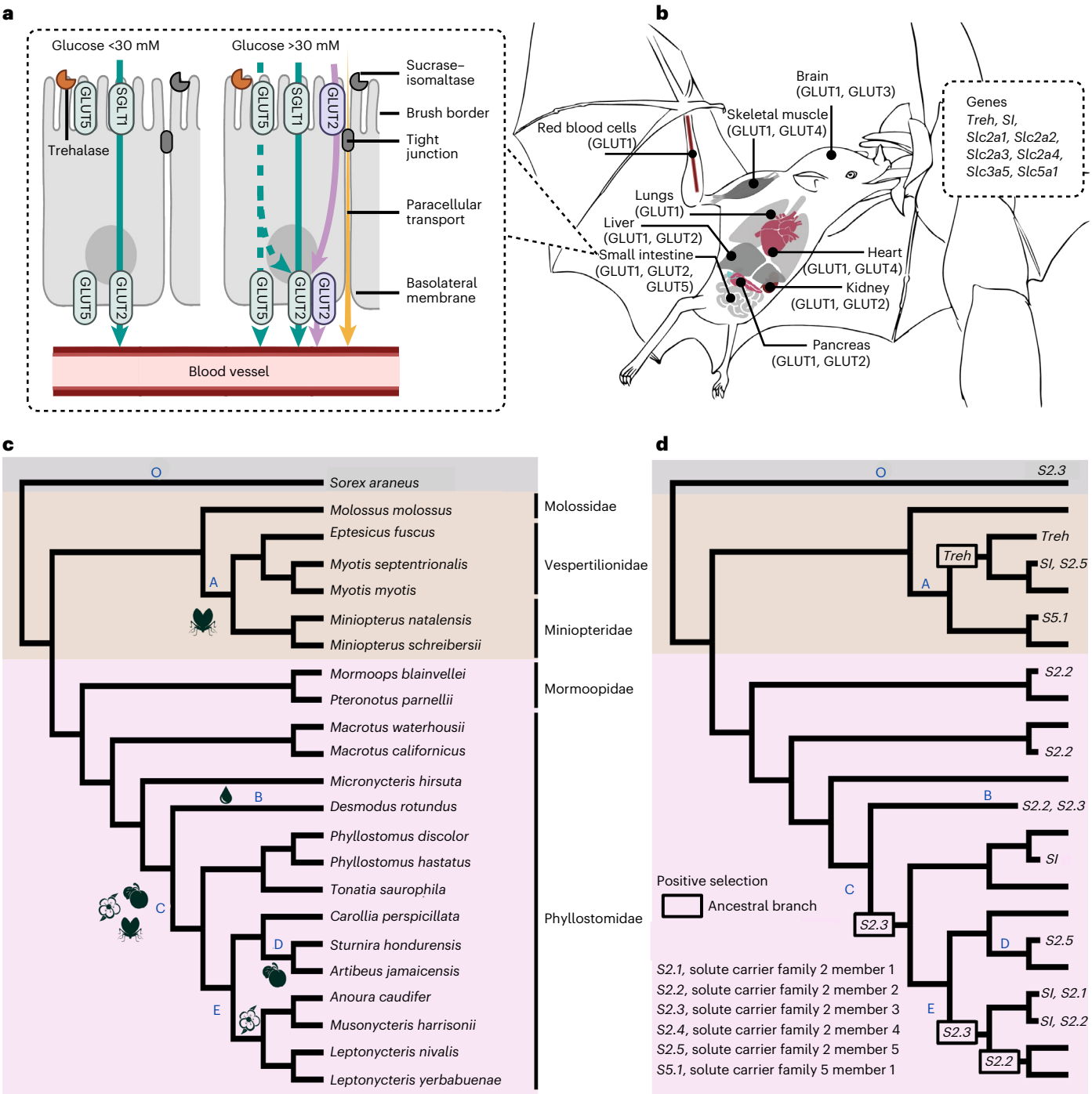

Fig. 2 | Molecular basis of sugar assimilation. a, Dietary sugar assimilation begins in the small intestine, along the brush border of enterocytes, where dietary enzymes TREH, trehalase, and SI, sucrase–isomaltase, are located. Glucose transporters (SLC2A2/GLUT2 and SLC2A5/GLUT5), sodium-glucose co-transporter (SGLT1) and paracellular transport determine the rate of glucose absorption into the bloodstream under low (<30 mM) and high (>30 mM) glucose concentrations. While GLUT5 is primarily a fructose transporter, it has the capacity to transport glucose[1,2]. **b**, Glucose transporters move glucose from the bloodstream into specific tissues. The genes include: *Treh*, *SI*, *Slc2a1*, *Slc2a2*, *Slc2a3*, *Slc2a4*, *Slc2a5* and *Slc5a1*. **c**, Species topology and foraging data follow Rojas et al. 2018. Insect-feeding branch leading to vesper and *Miniopterus* bats (A), blood-feeding (B), ancestral branch towards omnivores (C), obligate fruit eating (D) and nectarivore ancestral branch (E). **d**, Exploratory positive selection tests were performed using aBSREL with Holm–Bonferroni correction. Duodenal-enriched genes ($P < 0.01$) are shown across ancestral and extant Neotropical bats, using shrew as an outgroup (O).

we performed unbiased branch-site tests to identify episodic positive selection on orthologous gene sequences (Extended Data Table 4). While positive selection suggests advantageous genetic changes, it remains challenging to relate selection signatures to functional adaptation. In contrast, proteins possess distinct three-dimensional configurations intricately associated with their functions. Therefore, we modelled proteins from genes showing signatures of positive selection using Alphafold[59] and performed phylogenetically informed pairwise comparisons with Foldseek[60]. We interpret the predicted structural changes in the protein based on known experimental evidence to suggest potential functional alterations resulting from positive selection in gene sequences.

https://doi.org/10.1038/s41559-024-02485-7

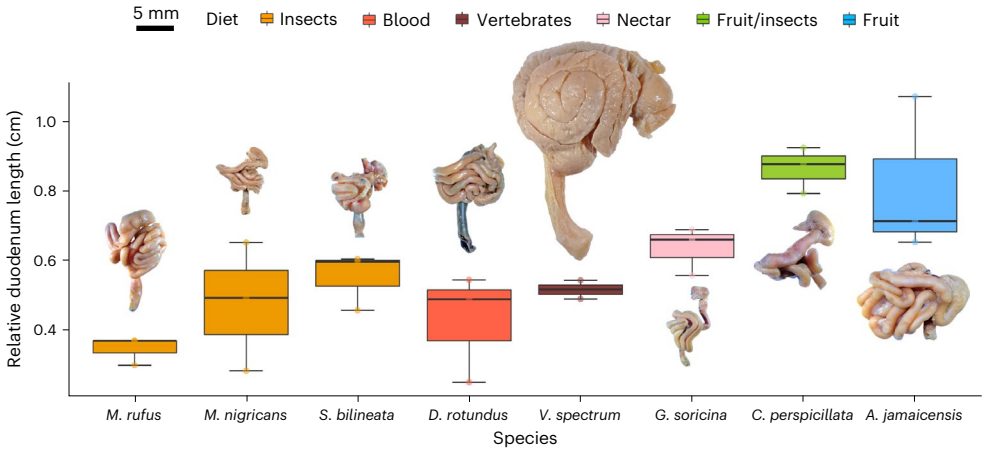

Fig. 3 | Relative length of duodenum associated with gastrointestinal tract morphology from eight bat species with different diets. Duodenum length relative to torso length in each species (shoulders to rump). *S. bilineata*, insectivorous; *M. nigricans*, insectivorous; *M. rufus*, insectivorous; *D. rotundus*, haematophagous; *V. spectrum*, carnivorous; *C. perspicillata*, omnivorous; *A. jamaicensis*, frugivorous; *G. soricina*, nectar-eating bat. Three biological replicates per species are reported, except for *V. spectrum* with two individuals. In the boxplots, the centre line represents the median, the limits or hinge are the first and third quartiles (the 25th and 75th percentiles), the whiskers extend to the largest and smallest value no further than 1.5× interquartile range) and the points represent the individual data. In general, species with fruit and nectar diets tend to have longer duodenum than the blood, meat and insect-eating species.

We identified positive selection signatures in the trehalase gene (*Treh*) along the ancestral branch of vespertilionids (Fig. 2d, branch A) and the *Eptesicus* branch, indicating possible adaptations to insectivorous diets. Surprisingly, the sucrase–isomaltase gene (*SI*) and transporter gene *Slc2a5* showed selection in the vespertilionid lineage *Myotis*. Comparisons of predicted protein structures revealed alterations to functional domains (Extended Data Fig. 5), which are known to affect sucrose tolerance and sugar absorption[61,62]. Perhaps these molecular changes contribute to the heightened sucrose assimilation observed in *Myotis* (Fig. 1a).

We also found positive selection on the *SI* gene in omnivore *Phyllostomus* and the nectar bats *Musonycteris harrisonii* and *Anoura caudifer* (Fig. 2d) accompanied by structural changes to the sucrase domain of the predicted *SI* structure (Extended Data Fig. 5). While *Phyllostomus* (Fig. 2c, branch C) showed limited glucose assimilation from digested sucrose (Fig. 1a), they have the potential for elevated sucrase activity and sucrose assimilation[34]. This suggests that the sucrase domain may facilitate dietary expansion to omnivory in *Phyllostomus*, allowing them to respond to seasonal changes in food availability. In nectar bats, it is expected for *SI* expression to increase[34,63], which increases blood glucose levels after consuming sucrose (Fig. 1a).

For glucose transporters, the vampire bat *Desmodus rotundus* (Fig. 2d, branch B), the ancestral branch leading to the Mexican nectar bat genus *Leptonycteris* and *M. harrisonii* (Fig. 2d, branch E) showed signatures of selection in gene *Slc2a2*. The vampire bat is renowned for its proficiency in running to hunt, and the Mexican nectar bats are known to undergo seasonal migrations to find flowering plants[64], which are metabolically expensive behaviours[65,66]. It is possible that the signatures of selection on *Slc2a2* might reveal functional adaptations related to assimilating glucose (Fig. 1a). When comparing predicted structures of GLUT2 (Extended Data Fig. 5), we observed changes in the ICH5 domain. This domain is post-translationally modified in the pancreatic beta cells to stabilize glucose sensing[67]. The observed domain change may possibly contribute to vampire bats and nectar bats having low levels of pancreatic beta cell release of insulin in response to glucose[46,68], conserving glucose energy for exercise.

We detected positive selection in the neuron-enriched *Slc2a3* gene (Fig. 2d) in the vampire bat *D. rotundus* (Fig. 2c, branch B), the ancestral branch leading to plant eating (Fig. 2c, branch C) and in the ancestral branch leading to nectar eating (Fig. 2c, branch E). The brain predominantly uses glucose as its main energy source, facilitated by the GLUT3 transporter known for its strong glucose affinity, especially during instances of low blood glucose levels, such as during fasting[69]. Positive selection on *Slc2a3* might relate to the evolution of expanded foraging variety and may have functional consequences in brain metabolism, as suggested by others[70,71]. The extent and location of structural change of GLUT3 is similar in the vampire bat and the nectar bat, relative to their closest outgroup relative *P. parnellii* (Extended Data Fig. 5). Possibly, these predicted structural changes in known binding site and transmembrane transport domains reflect similar functional changes to GLUT3 in these groups. From previous studies, we know vampire bats and nectar bats are unable to meet their metabolic demands with glucose released from liver glycogen stores, leading to a higher fasting intolerance[68,72], which may have resulted in positive selection for GLUT3 to protect the brain against such metabolic stress.

In the ancestral branch leading to fruit-eating species, we observed no significant molecular adaptations, corroborating a recent study on ancestral molecular evolution in Neotropical bats[73]. However, we observed a potential molecular adaptation related to glucose and fructose absorption in the genus *Sturnira* (Fig. 2c, branch D). We detected positive selection on *Slc2a5* together with structural changes in SLC2A5 in at least two domains known to affect nutrient transport (Extended Data Fig. 5) that might explain the distinctive in vivo blood glucose levels observed in *Sturnira* after sucrose ingestion (368 mg dl^{-1}), a pattern not observed in other fruit bats (Fig. 1a).

Intestine anatomy

We next investigated anatomical features of the small intestine, particularly the duodenum, where most glucose absorption occurs[74–76]. Consequently, the absorption through the duodenum represents the immediate pathway that glucose follows to reach the blood before reaching the jejunum or ileum. Since glucose assimilation did not show a phylogenetic signal, intestinal traits are more likely to be related to diet than to evolutionary relationships. In comparison with humans, bats lack circular folds in their small intestine[77], a finding that was confirmed in our analysis. We also observed striking differences in the intestinal length among bat species (Fig. 3), consistent with historical observations[78]. Notably, we found a correlation between duodenum length and the proportion of dietary sugar. Bats with rich-sugar diets exhibited longer duodenum, suggesting anatomical adaptations to deal with increased sugars and plant material, such as fibre, as they

shifted from insectivory to omnivory/frugivory. However, nectar bats are not constantly consuming high fibre levels, increased amino acids or increased fatty acid quantities through their diets[79]. Instead, their diet mainly consists of water and a high concentration of sugar[80]. Thus, we posit that simple sugars play a significant role in the shift in duodenum length.

The intestine, with its specialized villi structures projecting into the gut lumen, plays a crucial role in the absorption of nutrients such as sugars, amino acids, fatty acids and vitamins[81,82]. These villi consist of specialized epithelial cells (enterocytes) and goblet cells[83] and vary in shape among bats (Fig. 4). Among the seven bat species examined, we observed common finger-like villi (Fig. 4d, no. 1 and no. 2), previously described pyramidal villi (Fig. 4d, no. 4) and zig-zag villi (Fig. 4d, no. 6)[77,84,85]. Additionally, we found villi shapes (Fig. 4d, no. 3 and no. 5) that, to our knowledge, have not been reported before. Across the duodenum and beginning of the jejunum, insectivorous bats exhibited finger-like villi, some of which had simple entrances along the border (Fig. 4d, black triangles). *Glossophaga* exhibited entrances and sometimes an additional 'gap' in the middle of the finger-like villi body (Fig. 4d, no. 3, blue triangle). Pyramidal-shaped villi (Fig. 4d, no. 4) were found in *Carollia*, *Artibeus* and some *Myotis* individuals, while zig-zag villi (Fig. 4d, no. 6) were mainly found in *Artibeus* and *Carollia*, with rare occurrences in *Myotis*. *Glossophaga* also displayed pyramidal and zig-zag villi but with more pronounced entrances along the entire length of the villi. We identified a novel villi type (Fig. 4d, no. 5), that we referred to as 'ruffled', in *Carollia* and *Myotis*, characterized by multiple crests and troughs along its perimeter. The villi were scaled to the same size and their perimeter was measured (Extended Data Fig. 3). We found that while finger-like villi showed a perimeter of 339.56 µm, zig-zag villi were 931.99 µm and pyramidal villi with a gap in the middle were 1124.73 µm. The diverse villi morphologies observed suggest functional adaptations aimed at increasing the absorptive area in bats' intestines.

Interestingly, the insectivorous *Myotis* exhibited higher sucrose assimilation compared with other insectivorous bats. We found evidence of positive selection for genes encoding SI and SLC2A5 as well as predicted changes to protein structure in the *Myotis* lineage. Additionally, we observed similar villi shapes in fruit, nectar and omnivorous bats. *Myotis* was traditionally considered a strict insectivore; however, Novaes et al. (2015) reported fruit consumption in a species of this genus[86]. This finding, along with predation on insects that feed on nectar, may be linked to similar trait evolution observed in bats with sugar-rich diets. Further ecophysiological investigations are necessary within this genus and within phyllostomidae insectivorous species that might also consume plant material.

After adjusting for body size, we found a greater exposed surface area of villi in the duodenum for bats with sugar-rich diets (*Artibeus*, *Glossophaga* and *Carollia*) compared with insectivorous and vampire bats (Fig. 4a). The variation in duodenum villi exposure, combined with the in vivo physiology data suggests that the increased absorptive area in the duodenum of bats with sugar-rich diets may contribute to enhanced glucose absorption (Fig. 1a). A similar pattern has been observed in the proximal intestine of the distantly related frugivorous megabat *Epomophorus wahlbergi*[87,88].

Using transmission electron microscopy (TEM), we visualized the enterocytes and their microvilli in bats. We measured individual enterocytes, defined as the distance between tight junctions, and quantified the number of microvilli per enterocyte. Our analysis showed that bats with sugar-rich diets, particularly *Glossophaga* and *Artibeus*, had a higher number of enterocytes (Fig. 4b) and microvilli (Fig. 4c) compared with insect and vampire bats, especially compared with *Molossus*. The microvilli pattern observed in Neotropical bats aligns with discoveries in Paleotropical bats, despite their divergence in the early Eocene. Paleotropical insect eaters have smaller and fewer microvilli, while Paleotropical fruit bats have longer and more abundant microvilli[87,88]. The increased number of enterocytes suggests enhanced paracellular absorption between intestinal cells, as previously found in studies[89–92], contributing to the rise in blood glucose levels (Fig. 1a). In addition, the increase in microvilli provides greater space for glucose transporters and digestive enzymes along the brush border[93]. These results indicate that bats have varying intestinal absorption capabilities, which broadly relate to diet. For example, in nectar and fruit-eating bats, the numerous microvilli could increase the density of SI and apical transporters (SLC5A1, SLC2A2 and SLC2A5), thus facilitating the absorption of glucose, resulting in increased blood glucose levels to different degrees within the same diet type (Fig. 1a). This hypothesis would fit with observations made on the increased levels of the sucrase enzyme expression in nectar and fruit-eating bats[34].

Molecular mechanism of glucose absorption by transporters

We investigated the molecular activity underlying transcellular glucose absorption following a glucose meal and its impact on plasma glucose levels. We focused on the key molecular components of glucose absorption: Na^+-dependent glucose co-transporter, SGLT1 (*Slc5a1* gene), the apical solute carrier family member 2 glucose transporter, SLC2A2/GLUT2 (*Slc2a2* gene) and SLC2A5/GLUT5 (*Slc2a5* gene) (Fig. 2a) across seven bat species. The postprandial regulation of SI is not directly stimulated by glucose, as confirmed by quantitative polymerase chain reaction (qPCR) (Extended Data Fig. 4); therefore, we did not investigate this further. Additionally, non-insect-feeding bats lack a functional trehalase enzyme[35], precluding further examination in these species.

We employed multiplexed, single-molecule hybridization chain reaction (HCR) RNA fluorescence in situ hybridization (FISH) (Fig. 5a) on fasted bats ($t = 0$) and bats that were fed ($t = 10$) a single dose of glucose (5.4 g kg^{-1}(ref. 22) body weight). We note here that we were unable to examine protein localization at the apical membrane or within vesicles due to epitope disruption caused by prolonged methanol storage. We investigated two species within each dietary category (Fig. 5b–i): *Pteronotus parnellii* ($n = 4$) and *Micronycteris minuta* ($n = 1$) for insect-eating bats, *Carollia perspicillata* ($n = 4$) and *Phyllostomus discolor* ($n = 1$) for omnivorous bats and *G. soricina* ($n = 4$) and *Anoura geoffroyi* ($n = 4$) for nectar-feeding bats. Additionally, we examined one fruit-eating bat species, *Artibeus jamaicensis* ($n = 2$). For these experiments, we also used a more specialized glucometer (AlphaTRAK 2.0) and obtained blood glucose readings of more than 750 mg dl^{-1} (Extended Data Table 4). These levels are, to our knowledge, the highest documented for any wild species feeding on a single sugar dose of glucose solution. While we had limited biological replicates for some species (<2), we were still able to observe a notable pattern in gene expression at the level of the enterocyte. Insectivorous and omnivorous bats showed a comparable gene expression response to glucose. However, bats with a diet rich in sugar displayed markedly distinct patterns. Nectar bats (Fig. 5h,i)) consistently displayed a high *Slc2a2* signal in both fasting and fed states, whereas the fruit bat *A. jamaicensis* exhibited the highest *Slc2a5* signal (Fig. 5c).

Next, we quantified the fluorescent signal intensity of each HCR probe within individual enterocytes (n_{ent}) along the mid-length of the villi (Fig. 6). Additionally, we performed qPCR with reverse transcription (RT–qPCR) to observe broad patterns in RNA expression in the duodenum (Extended Data Fig. 4 and Extended Data Table 5). After administering dietary glucose, the molecular response patterns closely resembled those observed in mouse studies[94]; although, variations were evident among bat species (Extended Data Fig. 5). In the insectivorous bat, *P. parnellii*, enterocytes responded with a $\log_2$ fold change of 1.8 ($n_{ent} = 40$; adjusted P (P_{adj}) = 7.50×10^{-10}) in *Slc5a1* expression, 1.1 ($n_{ent} = 40$; $P_{adj} = 0.001$) in *Slc2a2* expression and 2.6 ($n_{ent} = 37$; $P_{adj} = 4.13 \times 10^{-9}$) in *Slc2a5* expression, accompanied by an average rise of 148.2 mg dl^{-1} in their blood glucose levels ($n = 7$; Extended Data Table 4). Comparatively, the insect bat *M. minuta* had an average change of 174.7 mg dl^{-1} in blood glucose ($n = 3$; Extended Data Table 4), indicating increased expression in molecular activity.

https://doi.org/10.1038/s41559-024-02485-7

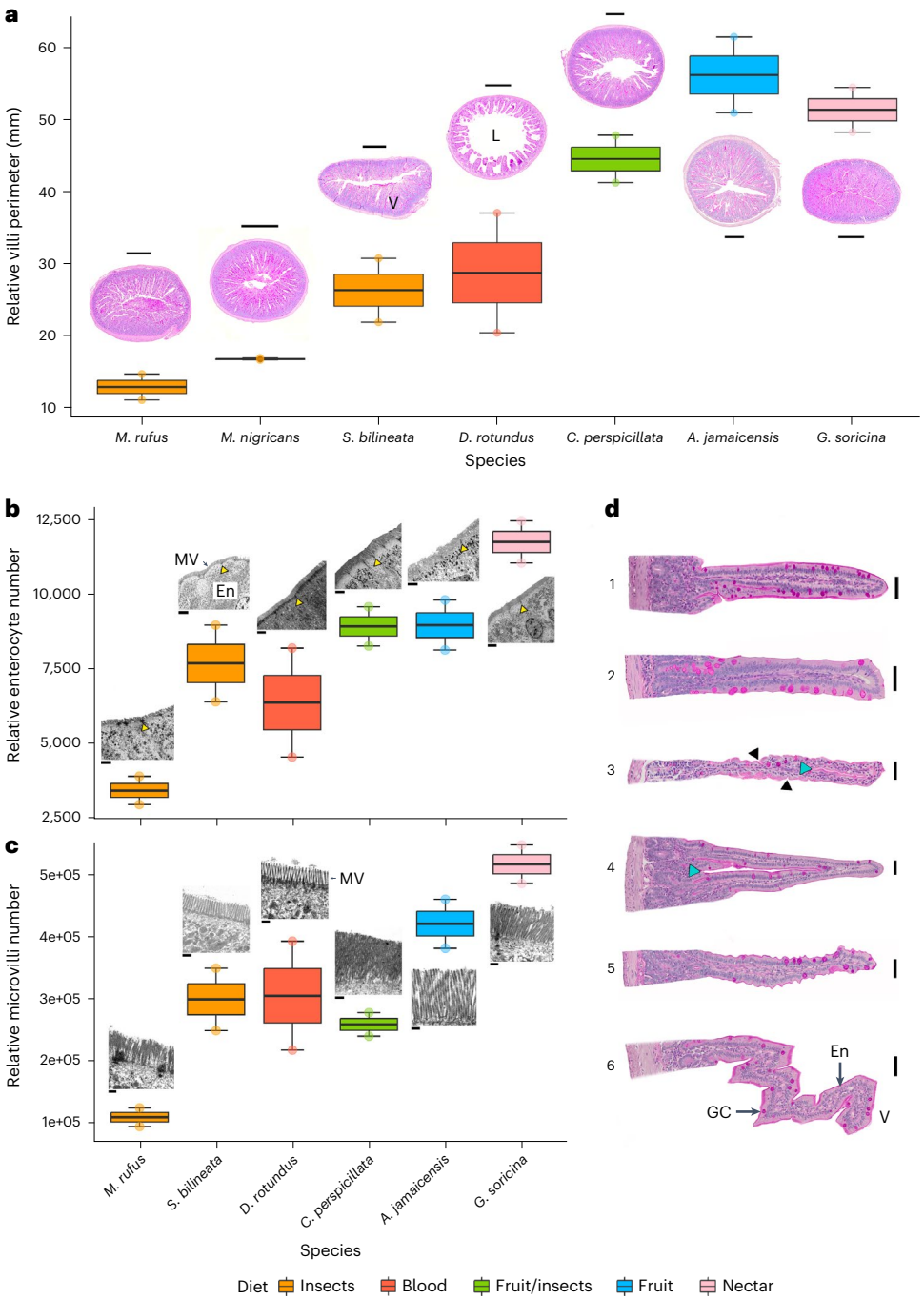

Fig. 4 | Histology of duodenum of bats with different diets. a, Relative villi perimeter across the duodenum related to cross sections for each species. **b**, Relative number of enterocytes along the duodenum related to TEM of the enterocytes and microvilli; **c**. Relative number of microvilli along the duodenum related to TEM of microvilli. **d**, Different types of villi in bats; no. 1 and no. 2, finger-like villi; no. 3, finger-like villi with entrances (black triangle) and gap (blue triangle); no. 4, arch-like villi with gap (blue triangle); no. 5, new villi 'ruffled'; and no. 6, zig-zag villi (nos. 1, 4 and 5 were extracted from *C. perspicillata*; no. 2 from *S. bilineata*; no. 3 from *G. soricina*; and no. 6 from *A. jamaicensis*). The species include: *M. rufus, S. bilineata, D. rotundus, C. perspicillata, A. jamaicensis* and *G. soricina*. Periodic acid–Schiff staining was performed for **a** and **d**. Scale bars, 250 µm (**a**), 2 µm (**b**), 0.4 µm (**c**), 20 µm (nos. 1–3 and 5, **d**) and 25 µm (nos. 4 and 6, **d**). The yellow triangles in **b** are pointing at tight junctions between enterocytes (En). MV, microvilli; V, villi; L, lumen; GC, goblet cells. Measurements were taken in different sections of the duodenum and are reported from one individual per species with two technical replicates for the histology section. For TEM, we had one individual and five technical replicates for enterocyte width and microvilli number, and the extrapolation to the whole duodenum was done for the two technical replicates from the histology sections. In the boxplots, the centre line represents the median, the limits or hinge are the first and third quartiles (the 25th and 75th percentiles), the whiskers extend to the largest and smallest value no further than 1.5× interquartile range and the points represent the individual data.

Meanwhile, *P. discolor* (omnivorous) demonstrated a blood glucose level change of 500 mg dl^{-1} from fasting levels ($n = 5$; Extended Data Table 4). It is worth noting that the expression level in response to glucose ($t = 10$) in this species is lower for *Slc5a1* ($n_{ent} = 18$; Extended Data Fig. 5a) compared with that observed in *P. parnellii* and the same for *Slc2a2* ($n_{ent} = 19$; Extended Data Fig. 5c) compared with *P. panellii*. The insect-eating, short-tailed fruit bat, *C. perspicillata*, exhibited an increase of 440.6 mg dl^{-1} in blood glucose levels ($n = 7$; Extended Data

https://doi.org/10.1038/s41559-024-02485-7

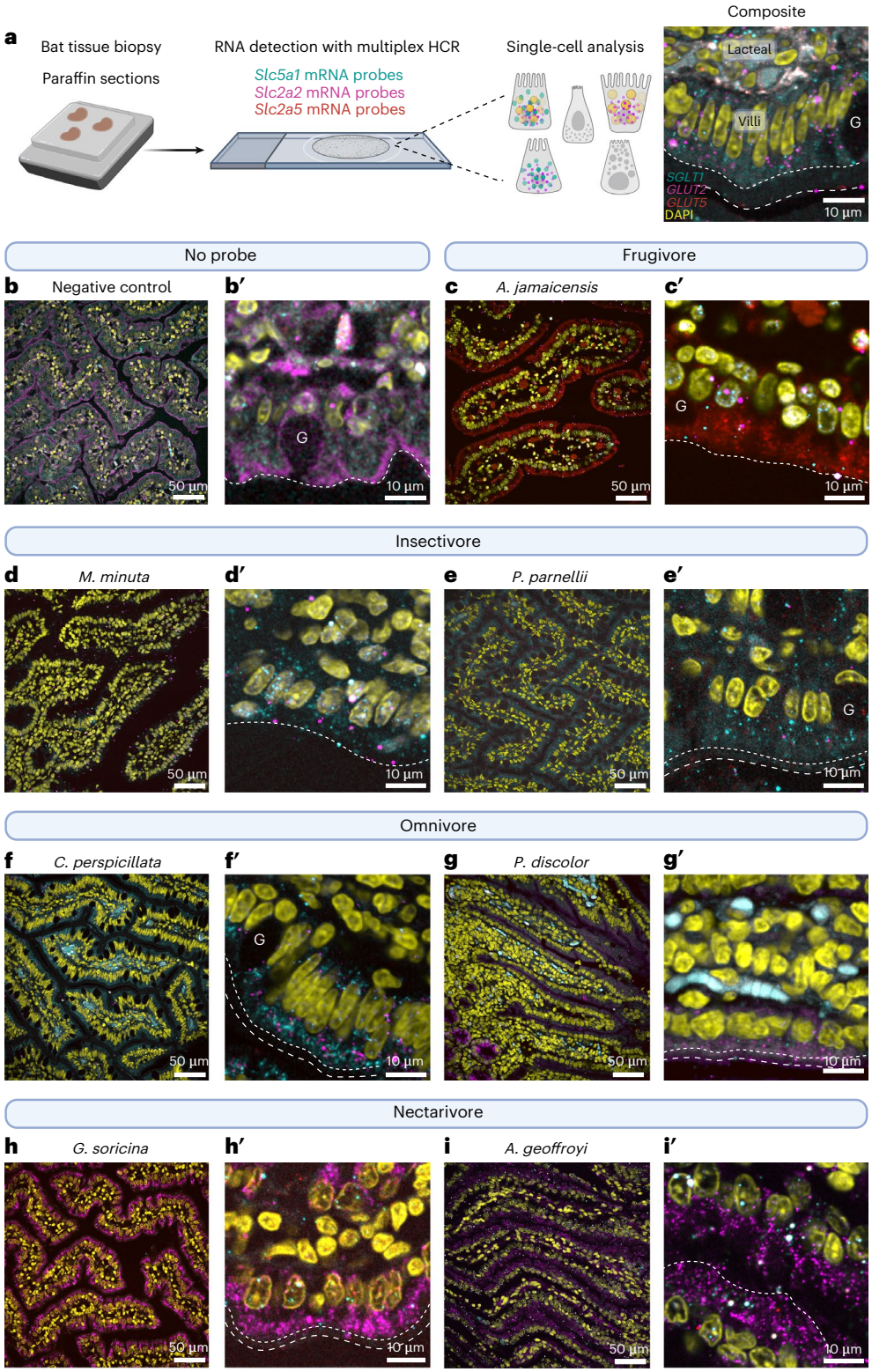

Fig. 5 | HCR RNA-FISH in the duodenum of bats from different diets. a, RNA expression is shown for bats fed a single dose (5.4 mg kg^{-1}body weight) of glucose. We performed HCR RNA-FISH with probe sets targeting messenger RNA (mRNA) for genes *Slc5a1*, *Slc2a2* and *Slc2a5* on fixed paraffin-embedded bat intestinal tissue and quantified the RNA fluorescent signal per enterocyte. An example composite image of the duodenum with all probes labelled with anatomical features is shown. The apical epithelial layer is shown with a fine-dotted line, and the microvilli brush border is shown with a dashed line; goblet cells are denoted by 'G'. Scale, 10 µm. **b**–**i**, 40× overview images of the intestinal villi for two omnivorous, two insectivorous, one frugivorous and two nectarivorous species. Scale, 50 µm. Negative control with no probes (**b**), fruit (*A. jamaicensis* ($n = 2$)) (**c**), insect (*M. minuta** ($n = 1$) (**d**) and *P. parnellii* ($n = 4$) (**e**)), omnivore (*C. perspicillata* ($n = 4$) (**f**) and *P. discolor* ($n = 1$) (**g**)), nectar (*G. soricina* ($n = 4$) (**h**) and *A. geoffroyi* (n = 4) (**i**) at $t = 10$ or *$t = 60$. **b**′–**i**′, Enlarged view of enterocytes along the villi. Scale bar, 10 µm. HCR probe sets are shown in cyan (*Slc5a1*), magenta (*Slc2a2*) and red (*Slc2a5*). DAPI (yellow) labels the cell nuclei. Bright, uniform and large circular spots (white) are background noise from amplifiers.

https://doi.org/10.1038/s41559-024-02485-7

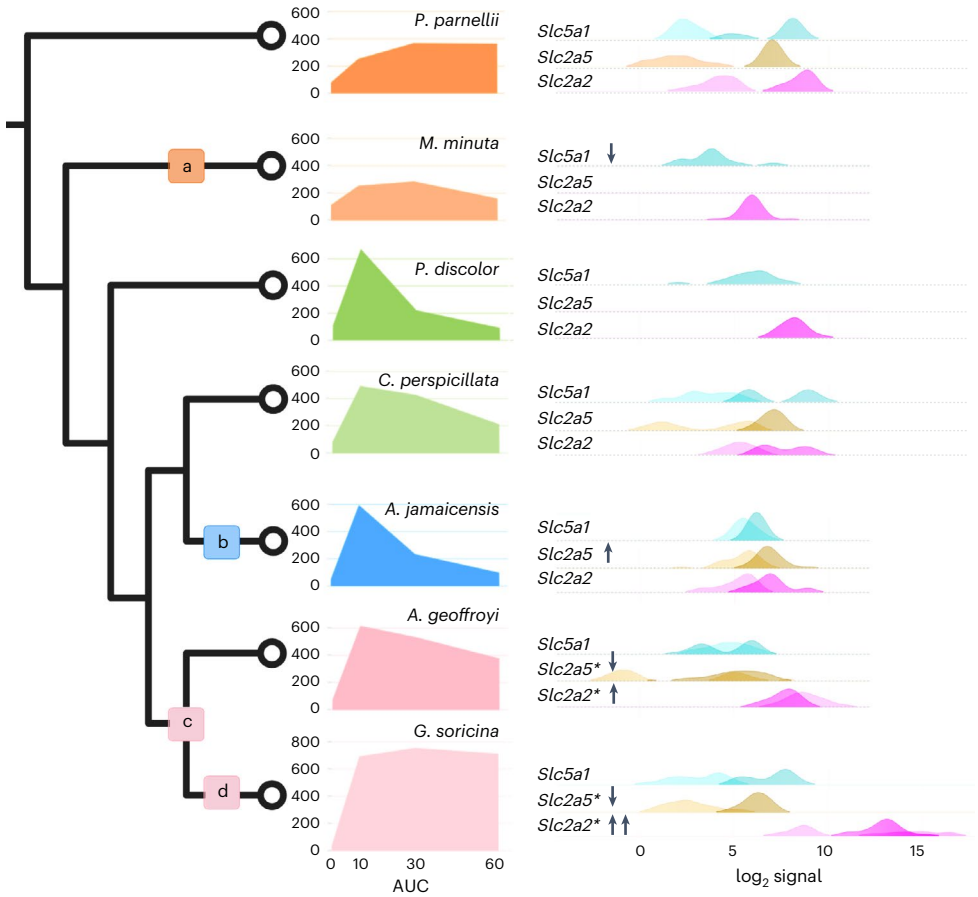

Fig. 6 | Parsimony-based evolutionary inferences of blood glucose levels in relation to gene expression. Average species blood glucose levels across 60 min (AUC) and change in gene expression 10 min after eating a 20% glucose solution. Most dietary guilds are represented by two species: insect, *P. parnelli* and *M. minuta*; fruit, *A. jamaicensis*; nectar, *A. geoffroyi* and *G. soricina*. *P. discolor* and *C. perspicillata* are omnivores incorporating large proportions of nectar or fruits, respectively, in their diet. Right: results of the single-cell image analysis taken from a minimum of 20 cells at fasted ($t = 0$) and fed ($t = 10$), presented as ridgeline density plots, coloured by the HCR probe and set as follows: *Slc5a1* (cyan), *Slc2a5* (yellow) and *Slc2a2* (magenta). The $\log_2$ values of fluorescent intensity are displayed for $t = 0$ in a lighter shade and $t = 10$ in a darker shade. Games–Howell pairwise comparisons with Holm–Bonferroni *P* adjustments were used to evaluate differences in gene expression across species (Extended Data Fig. 5). Shared gene expression responses (no notable differences) are taken as evidence for inheritance from a common ancestor. Significant gene expression differences among species (n_{ent}, $P < 0.001$) and blood glucose levels at 10-min post-feeding (Extended Data Table 4) are noted as apomorphies on the tree as follows: a: a decrease in *Slc5a1* in *M. minuta* ($n_{ent} = 23$) and blood glucose levels 200 mg dl^{-1} ($n = 3$), b: an increase in *Slc2a5* expression in *A. jamaicensis* ($n_{ent} = 43$) and blood glucose levels 600 mg dl^{-1} ($n = 6$), c: a decrease in *Slc2a5* expression and an increase in *Slc2a2* gene expression in *A. geoffroyi* ($n_{ent} = 76$) and *G. soricina* ($n_{ent} = 95$), with an increase in blood glucose (>600 mg dl^{-1}) and d: the highest expression of *Slc2a2* and the highest average reported blood glucose levels in *G. soricina* ($n = 7$, >750 mg dl^{-1}).

Table 4), a $\log_2$ fold change of 1.05 ($n_{ent} = 75$; $P_{adj} = 0.0001$) in *Slc5a1* expression, 0.468 ($n_{ent} = 72$; $P_{adj} = 0.001$) in *Slc2a2* expression and 1.11 ($n_{ent} = 74$; $P_{adj} = 5.27 \times 10^{-8}$) in *Slc2a5* (Extended Data Table 4), which is comparatively lower expression change than the insectivorous *P. parnellii* (Extended Data Fig. 5). RT–qPCR data further highlights that *P. parnellii* exhibits a broader change in glucose transporter activity in response to glucose compared with these more specialized phyllostomids (Extended Data Fig. 4). These data, summarized in Fig. 6, suggest that the dramatic rise in blood glucose levels in *P. discolor* and *C. perspicillata* can be primarily attributed to paracellular absorption.

The fruit-eating bat *A. jamaicensis* increased blood glucose levels by 483 mg dl^{-1} upon eating sugar ($n = 6$; Extended Data Table 4) but only displayed a $\log_2$ fold change of 0.006 in *Slc5a1* ($n_{ent} = 43$; $P_{adj} = 0.0001$), 0.350 in *Slc2a2* ($n_{ent} = 43$; $P_{adj} = 2.82 \times 10^{-4}$) and 0.294 in *Slc2a5* ($n_{ent} = 43$; $P_{adj} = 1.66 \times 10^{-3}$) (Extended Data Fig. 5). While expression changes were minimal, the initial fasting levels of *Slc5a1* and *Slc2a5* were significantly higher than those in *P. parnellii* ($P_{adj} = 0.001$ and $P_{adj} = 5.60 \times 10^{-7}$) and *C. perspicillata* ($P_{adj} = 5.67 \times 10^{-7}$ and $P_{adj} < 0.003$) (Extended Data Fig. 5), indicating that gene regulatory changes, in addition to paracellular absorption, may explain some of the rapid increase of blood glucose levels during the first 10 min interval of *A. jamaicensis* (Fig. 6). The nectar specialists, *A. geoffroyi* and *G. soricina*, showed the highest blood glucose change of 639.4 mg dl^{-1} ($n = 7$) and 659.2 mg dl^{-1} ($n = 7$), respectively (Extended Data Table 4). These two species showed significantly elevated expression in *Slc2a2* ($n_{Ag} = 37$, $n_{Gs} = 40$; $P_{adj} = 4.7 \times 10^{-11}$) at fasting (Extended Data Fig. 5c) and the lowest $\log_2$ fold change in *Slc2a2*, −0.123 ($n_{ent} = 76$) and 0.109 ($n_{ent} = 95$), respectively (Extended Data Table 4). Both nectar bat species also had lower expression ($n_{Ag} = 61$, $n_{Gs} = 93$; $P_{adj} = 1.19 \times 10^{-5}$) of *Slc2a5* compared with *P. panellii* (Extended Data Fig. 5b). These findings suggest a gain of function regulatory change in *Slc2a2* within enterocytes in relation to the rapid rise of blood glucose levels (Fig. 6).

When considering the broad patterns of blood glucose levels concerning the expression of intestinal transporters along the microvilli (Fig. 2a), we observe molecular apomorphies in transporter gene expression (Fig. 6). These differences may contribute to the diverse blood glucose patterns observed in the insectivore *M. minuta* (Fig. 6a), the frugivore *A. jamaicensis* (Fig. 6b) and the nectar bats (Fig. 6c,d). To relate how much and how long blood glucose levels remain elevated after the consumption of a glucose solution, we used a summary

measure of the overall glucose response, the area under the curve (AUC) (Fig. 6). Relative to the outgroup *P. parnellii*, a higher or lower AUC indicates a change in glucose assimilation. For example, *Slc5a1* expression is lower in *M. minuta* ($t = 60$), and we observe an AUC_{30-60} of 6,705 (Fig. 6a), in contrast to *P. parnellii*, which has higher expression of *Slc5a1* and an AUC_{30-60} of 9,630, indicating a diminished transfer of glucose through *Slc5a1* in *M. minuta* from the intestinal lumen to the bloodstream. Comparatively, the expression levels of transporter genes for *P. discolor* ($n = 5$; AUC_{0-10} of 3,312) and *C. perspicillata* ($n = 7$; AUC_{0-10} of 2,828) were lower to those of *P. parnellii* (AUC_{0-10} of 1,368). Since the expression in each enterocyte is lower in *P. discolor* and *C. perspicillata*, the rise in blood glucose levels is probably the result of an increase in the number of enterocytes made possible by an elongation of the duodenum (Fig. 3) and an expansion of the villi perimeter (Fig. 4a), which allows for more paracellular absorption[89–92]. On the contrary, *A. jamaicensis* enterocytes have an increase in *Slc5a1* ($n_{ent} = 43$) and *Slc2a5* ($n_{ent} = 43$) expression (Extended Data Fig. 5) and an AUC_{0-10} of 2973 (n = 6; Extended Data Table 4). The increased expression of glucose transporters may contribute to the rise in blood glucose levels, given that *A. jamaicensis* exhibits similar enterocyte numbers as *C. perspicillata* (Fig. 4b). The regulatory changes may be an apomorphic molecular change in the genus *Artibeus* (Fig. 6b) or it may be a plesiomorphic change in the subfamily Stenordermatidae, a specialized group of fruit-eating bats. It is worth mentioning that *Sturnira's* molecular adaptations to SLC2A5 (Fig. 2 and Extended Data Fig. 5e) might have been facilitated by the consistent usage of this molecular transport system. While fruit-eating bats have increased *Slc2a5*, nectar bats have decreased it, instead depending extensively on *Slc2a2* to increase blood glucose levels (Fig. 6c,d). The changes in the timing of *Slc2a2* and the amount of *Slc2a2* and *Slc2a5* expression probably reflect molecular plesiomorphies in the nectar bat subfamily Glossophaginae (Fig. 6c). A possible molecular apomorphy is represented by the excessively elevated levels of *Slc2a2* within the genus *Glossophaga* (Fig. 6d). Correspondingly, *A. geoffroyi* (AUC_{0-10} of 3,842) and *G. soricina* (AUC_{0-10} of 3,636) have extremely high blood glucose levels (average >700 mg dl^{-1}; Extended Data Table 4) compared with other bats.

This study demonstrates the first case of persistent intestinal *Slc2a2* expression found in a non-pathologic state in mammals. A comparable observation has been reported in the ruby-throated hummingbird, providing a notable example of convergent evolution[95]. The increase in *Slc2a2* expression also exemplifies repeated evolution towards a diet with a high sugar proportion, a molecular trait observed in Paleotropical fruit bats such as *Rousettus leschenaultia* and *Cynopterus sphinx*[96], which have maximum blood glucose levels between 430 and 490 mg dl^{-1}. These paleotropical species, along with neotropical bats such as *Carollia*, *Artibeus* and *Anoura*, were found to possess an 11-base pair deletion in the proximal promoter of the *Slc2a2* gene[96], predicted to disrupt the transcriptional repressor ZNF354C, thereby enhancing gene activity. The authors found an increase in the expression of liver *Slc2a2* in paleotropical fruit bats[96]. While we did not observe a prominent increase in *Slc2a2* expression at the level of the enterocyte in neotropical fruit bats, it might be increased in the liver cells. This alteration might explain their ability to rapidly clear blood glucose (Fig. 1a) and their increased capacity to store liver glycogen compared with nectar bats[72,97]. Future studies on tissue-specific gene regulation are needed to uncover mechanisms of evolutionary change across species.

Given the high glucose concentration present in nectar and their extremely high postprandial glucose levels, our study suggests that the distinctive expression pattern of *Slc2a2* is unique to nectarivorous bats (Fig. 6c). The permanent presence of apical *Slc2a2* might result from defective insulin action, as insulin typically triggers the internalization of GLUT2 (*Slc2a2* gene) to slow down sugar uptake and prevent high blood glucose levels after a sugar meal[98]. This is in line with the fact that nectar-feeding bats need to absorb high quantities of glucose to fuel their energetic requirements for hovering flight[43,99,100] and the hypothesis about additional mechanisms, complementary to insulin, to regulate glucose homoeostasis[22,44,45]. The magnitude of postprandial hyperglycaemia observed in nectar bats provides strong evidence that the adaptation towards nectar feeding has primed the duodenum for immediate and enhanced dietary sugar absorption, combining paracellular absorption with molecular absorption. The molecular metabolic adaptation is further supported by the permanent apical expression of *Slc2a2* associated with obesity and diabetes, conditions characterized by elevated blood glucose levels, insulin resistance and an increase in villous surface area[101–103]. Therefore, the long-term dietary adaptation to excess sugar consumption required the modification of the fundamental regulation of glucose absorption at the enterocyte level involving transporter trafficking in addition to the well-known paracellular absorption mechanism.

Conclusion

In our investigation into the metabolic adaptations across more than 29 bat species with diverse diets, we found higher assimilation of glucose and sucrose in nectarivorous, frugivorous and certain omnivorous bats, whereas insectivorous and omnivorous bats exhibited greater trehalose assimilation. Intriguingly, no insectivorous bat showed sugar absorption and assimilation as rapid and extensive as bats with sugar-rich diets. The observed variations in metabolic phenotypes are intricately linked to distinct adaptations in digestive morphology, including alterations in intestinal length, exposed villi and microvilli. Bats with sugar-rich diets exhibited a longer duodenum and higher numbers of enterocytes and microvilli along the initial section of the small intestine. These features suggest an enhanced capability for glucose absorption in bats with sugar-rich diets. Moreover, our study identifies key genetic traits associated with efficiently extracting maximal glucose energy from diet. Positive selection is evident in genes encoding for sucrase–isomaltase and glucose transporters in nectar and omnivorous bats and on a fructose transporter in a fruit bat. Structural comparisons of these proteins further elucidate the impact of amino acid substitutions on their functional roles, which may change enzymatic reaction speed or the affinity of glucose to transporters. Notably, our investigation extends beyond genetic traits to explore shifts in gene expression within single enterocytes along the brush border of the duodenum. This detailed examination of transporters SLC2A2/GLUT2 (*Slc2a2*), SLC2A5/GLUT5 (*Slc2a5*) and SLC5A1/SGLT1 (*Slc5a1*) unveils a nuanced interplay in response to dietary glucose. Across most bat species examined, there is a conserved expression response of sugar assimilation genes to glucose per enterocyte, so gut morphology appears to be the primary driver for glucose assimilation differences. As bats must limit gut size due to the constraints imposed by flight, their guts' microanatomy gets modified. It could also be that the structural changes we have documented make each transporter more efficient while keeping gene expression the same. However, the continuous expression of *Slc2a2* encoding for glucose transporter GLUT2 was exclusive to nectar bats, indicative of enhanced glucose receptivity. This interplay between physiology and ecology over evolutionary time illuminates the intricate adaptive mechanisms that underlie diet evolution in bats.

Methods

Our research complies with all relevant ethical regulations. The study protocol was approved by the Institute Board Committee Scientific Advisory Panel and the Institutional Animal Care and Use Committee at the Stowers Institute for Medical Research. The fieldwork was made under the permit of the National Authority of Environmental licences and the Ministry of Environment and Sustainable Development of Colombia, Resolution 1070, 28 August 2015, a Special Game licence from the Republic of Trinidad and Tobago Wildlife Section, Forestry Division, Ministry of Agriculture, Land and Marine Resources (2022)

and permit R-014-2022-OT-Conagebio from the Costa Rica National Commission for Biodiversity Management Division, Ministry of Environment and Energy (2022).

Field work

Bats were captured between June 2019 and December 2020 in 11 localities of the dry tropical forest ecosystem in the department of Valle del Cauca, Colombia, some within the Dry Tropical Project from the Institute for Research and Preservation of the Cultural and Natural Heritage of Valle del Cauca. To catch species with different food preferences (frugivores, insectivores, nectarivores, omnivores and haematophages), we opened mist nets between 18:00 and 24:00. In some instances, bats were manually captured in their refuge. Each individual was taxonomically identified, and their weight, age, sex, reproductive status and diet type were recorded. We also include species captured in Trinidad and Tobago as well as Costa Rica under an approved Institutional Animal Care and Use Committee from the Stowers Institute for Medical Research. We acknowledge that the bat's diet is more a continuum rather than static categories; however, for analysing the data, we grouped species according to their food preference and morphological adaptations for the consumption of the food resources[78,104–106]. In this way, the species of the genera *Artibeus*, *Dermanura*, *Uroderma* and *Sturnira* are considered frugivores; *Carollia* and *Phyllostomus* omnivores; *Glossophaga*, *Choeroniscus* and *Lonchophylla* nectarivores; *Desmodus* haematophagous; *Vampyrum* a carnivore; and *Saccopteryx*, *Peropteryx*, *Myotis*, *Molossus* and *Pteronotus* insectivorous. We include in vivo physiology data for 79 individuals with a preference for fruits, 55 omnivorous bats, 23 with a preference for nectar, 27 for insects, 14 for blood and 2 carnivorous bats (Extended Data Table 1). Juvenile individuals and pregnant or lactating females were excluded from the study due to high energy requirements and physiological changes during these stages, compared with non-pregnant or non-lactating adult individuals[107,108].

Oral glucose tolerance tests

After identification, bats were fed a 20% sugar solution and subsequently subjected to a period of fasting for 10–12 h. After fasting, each bat was fed a bolus of sugar (5.4 g $kg^{-1}$of body weight) as previously established by Kelm et al.[22]. Individual bats were only fed one type of sugar (glucose, sucrose or trehalose). To determine blood glucose levels, a drop of blood was drawn from the forearm with a 30G lancet before the sugar bolus and 10, 30 and 60 min post-feeding. The blood was immediately measured using a GlucoQuick G30a glucometer (Diabetrics) with a 20–600 mg dl^{-1} range. The individuals corresponding to *Lonchophylla* and *Pteronotus* were captured in Costa Rica and Trinidad and Tobago in 2022, respectively (Extended Data Table 4). Their blood glucose levels were measured with an AlphaTRAK 2.0 glucometer (Zoetis) with a range of 20–750 mg dl^{-1}; however, the measurements above 600 mg dl^{-1} were treated as 600 measurements to match the rest of the data previously obtained with the more limited range glucometer.

The bats individually remained in cloth bags between readings. Finally, the bats were tagged, fed and released. In total, blood glucose was measured for 199 individuals from 29 species and five families: Phyllostomidae, Mormoopidae, Emballonuridae, Vespertilionidae and Molossidae (Extended Data Table 1).

General patterns of sugar assimilation curves. We proposed general curves (Fig. 1b) to describe the temporal pattern of assimilation of different sugars in Neotropical bats based on a 1-h glucose tolerance test. The glucose curves were classified according to the speed of sugar assimilation to facilitate the understanding of the behaviour of the curves. The 'fast' assimilation curve shows a peak of blood glucose levels only after 10 min of sugar ingestion, followed by a decrease in blood glucose levels. The 'medium' assimilation curve shows a peak of blood glucose levels 30 min after sugar ingestion followed by a decrease in blood glucose levels. The 'slow' assimilation curve shows a continuous increase in blood glucose levels until the final timepoint, with the maximum levels 60 min after sugar ingestion. Finally, the 'limited' assimilation curve shows blood glucose levels with little variation throughout the different timepoints of the test.

Statistical analysis

Blood glucose levels of all bats measured were grouped by species and plotted in R (Fig. 1). Afterward, we evaluated the phylogenetic signal for the assimilation of the various sugars by the Pagel λ index[47]. We measured assimilation as the area under the glucose tolerance curve corrected, that is, setting the base of the curve at the minimal blood glucose level recorded for the average measurements of each genera. Additionally, to test for the interactive effect of timepoints and food preferences on the assimilation of sugars, by considering various individuals per species and the non-independence due to shared evolutionary history among taxa, we implemented a Bayesian multi-level phylogenetic model in the brms R package[109]. This multi-level model includes a varying intercept over species (using an indicator variable for species) and a covariance matrix to specify the lack of phylogenetic independence, allowing the analysis of hierarchical biological data while incorporating evolutionary relationships among species. For statistical inference, we compared 95% credible intervals from the models between timepoints and food preference combinations. We calculated the phylogenetic correlations among species from an ultrametric tree using the vcv function of the ape R package[110]. For phylogenetic analyses, we used the species-level mammal phylogeny of Upham et al. (2019) (http://vertlife.org/phylosubsets/), so we downloaded a credible set of 10,000 trees for all taxa we have data on for sugar assimilation and computed the consensus tree with the averageTree function of the phytools R package[111]. We performed the analysis using R[112] 4.3.1.

Morphology and histology of the gastrointestinal tract

We extracted the gastrointestinal tract from individuals preserved in 70% ethanol from species obtained in previous studies on bats[31] obtained under the Wildlife Section, Forestry Division, Ministry of Agriculture, Land and Marine Resources (Republic of Trinidad and Tobago) permit number 1737 (2014). The species incorporated in this section were *G. soricina*, *A. jamaicensis*, *C. perspicillata*, *Molossus rufus* and *Saccopteryx bilineata*. Additionally, we included two species obtained from the University of Kansas (KU) Biodiversity Institute and Natural History Museum: *Myotis nigricans* (KU 134846) and *D. rotundus* (KU 100374) and one species obtained from the American Museum of Natural History (AMNH): *Vampyrum spectrum* (M-267445, 272936). Finally we added more individuals to the analysis from the AMNH (*A. jamaicensis* 7473; *C. perspicillata* 7458, 175795; M. rufus 178675, 178672; *S. bilineata* 184693, 149982; *M. nigricans* 175725, 175724; *D. rotundus* 175406, 239943). We measured the length of the duodenum by imaging the unfolded, stretched intestine of each species with a Canon EOS Rebel E7i. Then, we determined the length through the Fiji platform[113]—Image J 1.53f51—and compared relative intestine length as the gut length divided by torso length (shoulders to rump length). We used this measure to control body size due to our focus on the intestine and its location, without adding measures related to the length of the rostrum or the tail, which can vary across bat species and families.

We investigated the duodenum because it is the main segment of the small intestine responsible for glucose absorption, and in vertebrates, the amount of absorbed glucose decreases as it reaches the next intestinal segments[74,75]. The duodenum is the first section of the intestine from the end of the stomach–pylorus to the duodenojejunal flexure[114]. The duodenum was recognized by its greater diameter compared with the jejunum, the intestine segment after the duodenum. The jejunum was also investigated through histology; however, its length

could not be assessed due to the external similarity between the end of the jejunum and the start of the ileum (Extended Data Fig. 3).

For histological comparisons, we cut 0.5–1 cm sections of the duodenum. The gut tissues were embedded in paraffin, serially cross sectioned to 10 µm and stained with periodic acid–Schiff. All tissues were imaged using an Olympus slide scanner equipped with a 20× objective and exported as a TIFF image. Two sections with good morphology per individual were chosen for study. We measured the area of villi and lumen (VLA) in each cross section, and then, we delimited 1/10 of VLA to measure the well-preserved villi perimeter (VPSA) in this sample area (SA). We also measured the lumen area (LA) to calculate the total villi perimeter along the cross section. Then, we corrected the measurement for size differences among species by considering the cross-section perimeter (CSP) from the different species. Finally, we extrapolated the final value from villi exposed in the whole cross section, corrected by size, to the relative duodenum length, as shown in equation (1) (measures summarized in Extended Data Fig. 3a):

$$\text{Villi in duodenum (Vduo)} = (((\text{VPSA} \times (\text{VLA} - \text{LA}))/\text{SA})/\text{CSP}) \times \text{Relative length of duodenum.} \quad (1)$$

Summary statistics were visualized with boxplots in Figs. 3 and 4. Descriptive comparisons among species were based on species averages.

TEM

To look closer at the enterocytes and microvilli, we used TEM. We sectioned 0.5–1.0 cm of duodenum from some of the species mentioned above (Fig. 3). The samples were rehydrated and fixed in 50 mM sodium cacodylate (pH 7.4) containing 2.5% paraformaldehyde and 2% glutaraldehyde. The tissue segments were then post-fixed with 2% OsO_4 for 2 h, washed and stained with 1% aqueous uranyl acetate overnight. After dehydration with a gradient of ethanol, the samples were infiltrated and embedded into Epon resin. Ultrathin (80 nm) sections were cut with a Leica UC7 Ultramicrotome, collected onto slot copper grids and stained with 4% uranyl acetate in 70% methanol and Sato's triple lead solution. Sections were imaged using a Field Emission Instruments (FEI) transmission electron microscope at 80 kV using the DigitalMicrograph software.

To calculate the number of enterocytes in the duodenum, we measured the enterocyte width of five different cells from each species, and the average was extrapolated to the relative length of the duodenum by dividing the villi surface found in the duodenum by the enterocyte width average. In addition, for calculating the number of microvilli in the duodenum, we counted the number of microvilli in each of the five different enterocytes where we measured the width, and then, we multiplied the average microvilli value by the number of enterocytes. All the measurements were made with the Fiji platform—ImageJ 1.53f51.

Genomics

Genome assemblies for 22 Chiroptera species, which included representatives from each of the dietary groups, were downloaded from online sources (Extended Data Table 3a). Transcriptomes and proteomes for 16 species were obtained from the National Center for Biotechnology Information (NCBI) and Ensembl databases (Extended Data Table 3b). After filtering out genomic contigs less than 10 kb, we generated gene models using MAKER (v3.01.03) using the 16 transcriptomes and proteomes (plus SwissProt/Uniprot v2021_03) as 'EST evidence' and 'Protein Homology Evidence'. RepeatMasker (open-4.0.7 with DB version 20170127) was used by MAKER to identify mammalian repeats. Links to the versions of all publicly available data (genome assemblies, transcriptomes and proteomes) used by MAKER can be accessed on SIMRbase. Our SIMR bat models were assigned names derived from Uniprot[115] best hit with an e-value ≤1×10^{-5}. SIMR bat models are available for download and for browsing at https://simrbase.stowers.org/bats/data. Genome browsers were built using Jbrowse[116] and SIMRbase was built using Tripal[117].

Ortholog assignment and candidate gene identification

To relate the blood glucose tolerance assay to evolution, we identified genes involved in sugar assimilation, specifically from the gut absorption into the bloodstream. A short list of eight genes were identified as having biased function and expression in the duodenum using mouse ENCODE (NCBI Bioproject PRJNA66167) and human HPA (NCBI Bioproject PRJEB4337). Orthologs were assigned to the SIMR bat models with standalone Orthologous Matrix (OMA) (version 2.4.2) using three species included in the OMA FASTA database (April 2021), *Homo sapiens* (HUMAN), *Pteropus vampyrus* (PTEVA) and *Myotis lucifugus* (MYOLU). A gene is considered an ortholog if it is found in the same OMA ortholog group as a HUMAN candidate gene with appropriate HGNC identifiers (Extended Data Table 3).

Phylogenetic analysis of sugar related genes

Whole genome alignments of single-copy orthologs trimmed with trimAl v1.4.rev15 (ref. 118) from 22 SIMR bat models and two outgroups (Extended Data Table 3) and were used to generate a phylogenomic tree[119] using RaxML version 8.1.15 (PROTFAMMAUTO model). Our molecular phylogeny, which matches published species topologies[73,120–122], includes a broad taxonomic sampling, incorporating Miniopteridae, Vespertilionidae and Molossidae (Fig. 2, branch A). The resulting phylogeny was used for all exploratory selection tests of candidate genes along all branches (Extended Data Table 4). The tested DNA sequences were from single-copy orthologs found using OMA. For selection tests, we used the codon-based method measuring non-synonymous (dN) to synonymous nucleotide (dS) substitutions (the dN/dS metric, ω) with the tool HyPhy (hyphy.org). To identify branches under positive selection, aBSREL[56] was used.

Structural phylogenetics using Alphafold and Foldseek

Alphafold is a large scale language model used to impute protein structures from sequence[59]. We used Alphafold v2, which is available at https://github.com/google-deepmind/alphafold. With the protein structure, we then performed structural alignments with Foldseek[60], which can be downloaded at https://github.com/steineggerlab/foldseek. The metric for assessing the topological similarity of protein structure is the TM-score, which has the value in (0,1), where 1 represents a perfect match between two structures.

HCR RNA-FISH

Additional glucose tolerance tests (Extended Data Table 4) were performed on *P. parnellii* ($n = 7$) and *M. minuta* ($n = 3$, insect diet), *C. perspicillata* ($n = 7$, piper–insect diet), *A. jamaicensis* ($n = 6$, fig-fruit diet), *A. geoffroyi* ($n = 7$) and *G. soricina* ($n = 7$, nectar diet) and *P. discolor* ($n = 5$, insect–fruit–nectar diet) in April 2022 and April 2023 with permission from the Republic of Trinidad and Tobago. To determine blood glucose levels, a drop of blood was drawn from the forearm with a 30G lancet before the sugar bolus and 10 min post-feeding. The blood was immediately measured using an AlphaTRAK 2.0 glucometer (Zoetis) with a range of 20–750 mg dl^{-1} calibrated for cats (health range 120–300 mg dl^{-1}). Finally, the bats were euthanized ($n = 2$–4 per species), and the tissue was dissected, fixed and stored in 4% paraformaldehyde.

Fluorescently labelled HCR hairpins targeting SGLT1 (*Slc5a1*), GLUT2 *(Slc2a2)* and GLUT5 *(Slc2a5)* in fasted and fed bats were purchased from Molecular Technologies, and thrid generation HCR RNA-FISH was performed on 10 µm paraffin sections of the duodenum. Slides were deparaffinized and microwave antigen retrieval was applied at 95 °C for 15 min. A hydrophobic barrier was created using ImmEdge Hydrophobic Barrier PAP Pen (Vector laboratories) around the sections on a slide, and bleaching solution (3% H_2O_2, 5% formamide, 0.5× SSC)

was applied for 30 min under strong light-emitting diode light. Tissue sections were permeabilized with proteinase K (20 ug ml^{-1}) for 12 min at room temperature, washed with PBS five times, incubated in hybridization buffer for 30 min at 37 °C, and incubated in hybridization buffer containing probes at 37 °C for 16 h. Tissue sections were washed five times with the wash buffer for 5 min each, then two times in the 5× SSCT (5× SSC + 0.1% Tween 20). Fluorescently labelled HCR amplifiers were snap-cooled by heating at 95 °C for 90 s, cooling to room temperature for 30 min under dark conditions and added to the amplification buffer. Tissue sections were incubated in the amplification buffer for 30 min at room temperature and incubated in an amplification buffer containing amplifiers overnight at room temperature in a humid chamber under dark conditions. Slides were washed four times in 5× SSCT for 5 min each, stained with 4,6-diamidino-2-phenylindole (DAPI, 10ug ml^{-1}) in 5× SSCT for 30 min and then washed two times in 5× SSCT. Prolong gold (Invitrogen) was mounted, and slides were stored at 4 °C until imaging.

Image analysis

Images were taken on a Nikon Ti Eclipse with CSU-W1 spinning disk confocal microscope at 40× magnification. Image data for fluorescence intensity were $\log_2$ transformed for comparisons between timepoints within a species and across species. Two to three sections per individual with good morphology were chosen for study. For each section, five to ten cells were isolated for analysis. Fluorescence signals were quantified using threshold-based segmentation and spot detection (n = 17–55 cells per treatment per species) in FIJI. We performed Games–Howell pairwise comparisons using the 'ggstatsplot' function in R, with Holm–Bonferroni P adjustments for multiple comparisons (Extended Data Fig. 5).

qPCR

Total RNA was isolated from 3–5 mg flash frozen duodenum tissue from *Ptenonotus parnellii* ($n_{t=10}$ = 3, $n_{t=0}$ = 3), *C. perspicillata* ($n_{t=10}$ = 2, $n_{t=0}$ = 3), *A. jamaicensis* ($n_{t=10}$ = 2, $n_{t=0}$ = 1) *A. geoffroyi* ($n_{t=10}$ = 4, $n_{t=0}$ = 3) and *G. soricina* ($n_{t=10}$ = 3, $n_{t=0}$ = 1). RNA was extracted using Promega Maxwell RSC simplyRNA Tissue Kit. Quantification was performed using Qubit RNA High Sensitivity Assay Kit and quality was assessed using a 1% agarose gel stained with ethidium bromide. Downstream complementary DNA synthesis was performed using Applied Biosystems High-Capacity RNA-to-cDNA Kit using a programmed thermal cycler at 37 °C for 60 min, followed by a 5 min incubation at 95 °C, before cooling to 4 °C. The specific primer sequences used for target genes *sglt1 Slc5a1/sglt1*, *Slc2a2/glut2*, sucrase–isomaltase (*SI*) and reference gene *gapdh* are shown in Extended Data Fig. 4 and were ordered from Integrated DNA Technologies (IDT). Primer pair validation and experimentation were performed using QuantStudio 7 Pro Real-time qPCR platform and software. The data generated from qPCR were analysed using the $2^{-\Delta\Delta Ct}$ method[123] to assess variance in relative fold gene expression between *Slc5a1/sglt1*, *si* and *Slc2a2/glut2* against the housekeeping gene *gapdh*. For heat map visualization of normalized gene expression (ΔCt), the R package 'pheatmap' version 1.0.12 was used. Clusters are based on 'Euclidean' distance measures, also performed on the R package 'pheatmap'. Statistical analysis on fold gene expression changes (ΔΔCt) at t = 10 relative to t = 0 between species was evaluated with a one-way analysis of variance in GraphPad Prism 10.2.0 (Extended Data Table 5).

Reporting summary

Further information on research design is available in the Nature Portfolio Reporting Summary linked to this article.

Data availability

Original data underlying this manuscript can be publically accessed from the Stowers Original Data Repository at http://www.stowers.org/research/publications/LIBPB-2406. Original genome data can be found in Extended Data Table 3. Our Genome browsers are publically available here: https://simrbase.stowers.org/bats_sugar_assimilation. Source data are provided with this paper.

References

1. Pauli, J. N., Peery, M. Z., Fountain, E. D. & Karasov, W. H. Arboreal folivores limit their energetic output, all the way to slothfulness. *Am. Nat.* **188**, 196–204 (2016).
2. Tokita, M., Yano, W., James, H. F. & Abzhanov, A. Cranial shape evolution in adaptive radiations of birds: comparative morphometrics of Darwin's finches and Hawaiian honeycreepers. *Philos. Trans. R. Soc. B* **372**, 20150481 (2017).
3. Camacho, J. et al. Peramorphosis, an evolutionary developmental mechanism in Neotropical bat skull diversity. *Dev. Dyn.* **248**, 1129–1143 (2019).
4. Morris, Z. S., Vliet, K. A., Abzhanov, A. & Pierce, S. E. Heterochronic shifts and conserved embryonic shape underlie crocodylian craniofacial disparity and convergence. *Proc. R. Soc. B* **286**, 20182389 (2019).
5. Lyons, K., Dugon, M. M. & Healy, K. Diet breadth mediates the prey specificity of venom potency in snakes. *Toxins* **12**, 74 (2020).
6. Dobreva, M. P., Camacho, J. & Abzhanov, A. Time to synchronize our clocks: connecting developmental mechanisms and evolutionary consequences of heterochrony. *J. Exp. Zoolog. B* **338**, 87–106 (2022).
7. Yohe, L. R. et al. Ecological constraints on highly evolvable olfactory receptor genes and morphology in Neotropical bats. *Evolution* **76**, 2347–2360 (2022).
8. Sadier, A. et al. Bat teeth illuminate the diversification of mammalian tooth classes. *Nat. Commun.* **14**, 4687 (2023).
9. Deas, J. B., Blondel, L. & Extavour, C. G. Ancestral and offspring nutrition interact to affect life-history traits in *Drosophila melanogaster*. *Proc. R. Soc. B* **286**, 20182778 (2019).
10. Koyama, T., Texada, M. J., Halberg, K. A. & Rewitz, K. Metabolism and growth adaptation to environmental conditions in *Drosophila*. *Cell. Mol. Life Sci.* **77**, 4523–4551 (2020).
11. Karasov, W. H. & Caviedes-Vidal, E. Adaptation of intestinal epithelial hydrolysis and absorption of dietary carbohydrate and protein in mammals and birds. *Comp. Biochem. Physiol. A* **253**, 110860 (2021).
12. Riddle, M. R. et al. Genetic mapping of metabolic traits in the blind Mexican cavefish reveals sex-dependent quantitative trait loci associated with cave adaptation. *BMC Ecol. Evol.* **21**, 1–22 (2021).
13. Xiong, S. et al. Enhanced lipogenesis through Ppary helps cavefish adapt to food scarcity. *Curr. Biol.* **32**, 2272–2280.e6 (2022).
14. Fujisaka, S. et al. Diet, genetics, and the gut microbiome drive dynamic changes in plasma metabolites. *Cell Rep.* **22**, 3072–3086 (2018).
15. Karasov, W. H. & Douglas, A. E. Comparative digestive physiology. *Compr. Physiol.* **3**, 741 (2013).
16. Costa, D. P. & Ortiz, C. L. Blood chemistry homeostasis during prolonged fasting in the northern elephant seal. *Am. J. Physiol. Regul. Integr. Comp. Physiol.* **242**, R591–R595 (1982).
17. Tomasek, O., Bobek, L., Kralova, T., Adamkova, M. & Albrecht, T. Fuel for the pace of life: baseline blood glucose concentration co-evolves with life-history traits in songbirds. *Funct. Ecol.* **33**, 239–249 (2019).
18. Sparkman, A. M. et al. Convergence in reduced body size, head size, and blood glucose in three island reptiles. *Ecol. Evol.* **8**, 6169–6182 (2018).
19. Bennett, K. A., Turner, L. M., Millward, S., Moss, S. E. & Hall, A. J. Obtaining accurate glucose measurements from wild animals under field conditions: comparing a hand held glucometer with a standard laboratory technique in grey seals. *Conserv. Physiol.* **5**, cox013 (2017).

20. Saxton, M. W. et al. Serum plays an important role in reprogramming the seasonal transcriptional profile of brown bear adipocytes. *iScience* **25**, 105084 (2022).
21. Oriel, R. C., Wiley, C. D., Dewey, M. J. & Vrana, P. B. Adaptive genetic variation, stress and glucose regulation. *Dis. Model. Mech.* **1**, 255–263 (2008).
22. Kelm, D. H., Simon, R., Kuhlow, D., Voigt, C. C. & Ristow, M. High activity enables life on a high-sugar diet: blood glucose regulation in nectar-feeding bats. *Proc. R. Soc. B* **278**, 3490–3496 (2011).
23. Riddle, M. R. et al. Insulin resistance in cavefish as an adaptation to a nutrient-limited environment. *Nature* **555**, 647–651 (2018).
24. Reznick, J., Park, T. J. & Lewin, G. R. in *The Extraordinary Biology of the Naked Mole-Rat* (eds Buffenstein, R., Park, T. J. & Holmes, M. M.) 271–286 (Springer, 2021).
25. Gao, X. et al. The function of glucose metabolism in embryonic diapause of annual killifish. *Comp. Biochem. Physiol. Part D* **42**, 100965 (2022).
26. Chouchani, E. T. & Kajimura, S. Metabolic adaptation and maladaptation in adipose tissue. *Nat. Metab.* **1**, 189–200 (2019).
27. Bundgaard, A. et al. Metabolic adaptations during extreme anoxia in the turtle heart and their implications for ischemia-reperfusion injury. *Sci Rep.* **9**, 2850 (2019).
28. Neuweiler, G. *The Biology of Bats* (Oxford Univ. Press, 2000).
29. Arbour, J. H., Curtis, A. A. & Santana, S. E. Signatures of echolocation and dietary ecology in the adaptive evolution of skull shape in bats. *Nat. Commun.* **10**, 2036 (2019).
30. Price, S. A., Hopkins, S. S., Smith, K. K. & Roth, V. L. Tempo of trophic evolution and its impact on mammalian diversification. *Proc. Natl Acad. Sci USA* **109**, 7008–7012 (2012).
31. Camacho, J. et al. Differential cellular proliferation underlies heterochronic generation of cranial diversity in phyllostomid bats. *EvoDevo* **11**, 11 (2020).
32. Wyatt, G. R. & Kalf, G. F. The chemistry of insect hemolymph. *J. Gen. Physiol.* **40**, 833–847 (1957).
33. Baker, H. G., Baker, I. & Hodges, S. A. Sugar composition of nectars and fruits consumed by birds and bats in the tropics and subtropics. *Biotropica* **30**, 559–586 (1998).
34. Schondube, J. E., Herrera-M, L. G. & Martínez Del Rio, C. Diet and the evolution of digestion and renal function in phyllostomid bats. *Zoology* **104**, 59–73 (2001).
35. Jiao, H. et al. Trehalase gene as a molecular signature of dietary diversification in mammals. *Mol. Biol. Evol.* **36**, 2171–2183 (2019).
36. Zepeda Mendoza, M. L. et al. Hologenomic adaptations underlying the evolution of sanguivory in the common vampire bat. *Nat. Ecol. Evol.* **2**, 659–668 (2018).
37. Ingala, M. R. et al. You are more than what you eat: potentially adaptive enrichment of microbiome functions across bat dietary niches. *Anim. Microbiome* **3**, 82 (2021).
38. Santos, M., Aguirre, L. F., Vázquez, L. B. & Ortega, J. *Phyllostomus hastatus*. *Mamm. Species* https://doi.org/10.1644/0.722.1 (2003).
39. York, H. A. & Billings, S. A. Stable-isotope analysis of diets of short-tailed fruit bats (Chiroptera: Phyllostomidae: Carollia). *J. Mammal.* **90**, 1469–1477 (2009).
40. Protzek, A. O. P. et al. Insulin and glucose sensitivity, insulin secretion and β-cell distribution in endocrine pancreas of the fruit bat *Artibeus lituratus*. *J. Comp. Physiol. B* **180**, 627–634 (2010).
41. Ayala-Berdon, J., Rodríguez-Peña, N., García Leal, C., Stoner, K. E. & Schondube, J. E. Sugar gustatory thresholds and sugar selection in two species of Neotropical nectar-eating bats. *Comp. Biochem. Physiol. A* **164**, 307–313 (2013).
42. Ortega-García, S. & Saldaña-Vázquez, R. A. Synthesis of knowledge of the plant diet of nectar-feeding bats of Mexico. *Therya* **13**, 335–343 (2022).
43. Welch, K. C. Jr, Herrera M, L. G. & Suarez, R. K. Dietary sugar as a direct fuel for flight in the nectarivorous bat *Glossophaga soricina*. *J. Exp. Biol.* **211**, 310–316 (2008).
44. Welch, K. C. & Chen, C. C. Sugar flux through the flight muscles of hovering vertebrate nectarivores: a review. *J. Comp. Physiol. B* **184**, 945–959 (2014).
45. Peng, X. et al. Flight is the key to postprandial blood glucose balance in the fruit bats *Eonycteris spelaea* and *Cynopterus sphinx*. *Ecol. Evol.* **7**, 8804–8811 (2017).
46. Castro, D. L. J. et al. Insulin and glucose regulation at rest and during flight in a Neotropical nectar-feeding bat. *Mamm. Biol.* **101**, 987–996 (2021).
47. Pagel, M. Inferring the historical patterns of biological evolution. *Nature* **401**, 877–884 (1999).
48. Saldaña-Vázquez, R. A., Ruiz-Sanchez, E., Herrera-Alsina, L. & Schondube, J. E. Digestive capacity predicts diet diversity in Neotropical frugivorous bats. *J. Anim. Ecol.* **84**, 1396–1404 (2015).
49. Burant, C. F., Takeda, J., Brot-Laroche, E., Bell, G. I. & Davidson, N. O. Fructose transporter in human spermatozoa and small intestine is GLUT5. *J. Biol. Chem.* **267**, 14523–14526 (1992).
50. Mizuno, T. M., Lew, P. S. & Jhanji, G. Regulation of the fructose transporter gene Slc2a5 expression by glucose in cultured microglial cells. *Int. J. Mol. Sci.* **22**, 12668 (2021).
51. Navale, A. M. & Paranjape, A. N. Glucose transporters: physiological and pathological roles. *Biophys. Rev.* **8**, 5–9 (2016).
52. Veys, K. et al. Role of the GLUT1 glucose transporter in postnatal CNS angiogenesis and blood-brain barrier integrity. *Circ. Res.* **127**, 466–482 (2020).
53. Thorens, B. GLUT2, glucose sensing and glucose homeostasis. *Diabetologia* **58**, 221–232 (2015).
54. Gerhart, D. Z., Broderius, M. A., Borson, N. D. & Drewes, L. R. Neurons and microvessels express the brain glucose transporter protein GLUT3. *Proc. Natl Acad. Sci USA.* **89**, 733–737 (1992).
55. Richter, E. A. & Hargreaves, M. Exercise, GLUT4, and skeletal muscle glucose uptake. *Physiol. Rev.* **93**, 993–1017 (2013).
56. Smith, M. D. et al. Less is more: an adaptive branch-site random effects model for efficient detection of episodic diversifying selection. *Mol. Biol. Evol.* **32**, 1342–1353 (2015).
57. Pond, S. L. K., Frost, S. D. W. & Muse, S. V. HyPhy: hypothesis testing using phylogenies. *Bioinformatics* **21**, 676–679 (2005).
58. Pond, S. L. K. et al. HyPhy 2.5—a customizable platform for evolutionary hypothesis testing using phylogenies. *Mol. Biol. Evol.* **37**, 295–299 (2020).
59. Jumper, J. et al. Highly accurate protein structure prediction with AlphaFold. *Nature* **596**, 583–589 (2021).
60. van Kempen, M. et al. Fast and accurate protein structure search with Foldseek. *Nat. Biotechnol.* **42**, 243–246 (2023).
61. Hoffmann, W. & Hauser, F. The P-domain or trefoil motif: a role in renewal and pathology of mucous epithelia? *Trends Biochem. Sci* **18**, 239–243 (1993).
62. Quistgaard, E. M., Löw, C., Moberg, P., Trésaugues, L. & Nordlund, P. Structural basis for substrate transport in the GLUT-homology family of monosaccharide transporters. *Nat. Struct. Mol. Biol.* **20**, 766–768 (2013).
63. Yasutake, H., Goda, T. & Takase, S. Dietary regulation of sucrase–isomaltase gene expression in rat jejunum. *Biochim. Biophys. Acta BBA* **1243**, 270–276 (1995).
64. Arita, H. T. & Santos-del-Prado, K. Conservation biology of nectar-feeding bats in Mexico. *J. Mammal.* **80**, 31–41 (1999).
65. McNab, B. K. Energetics and the distribution of vampires. *J. Mammal.* **54**, 131–144 (1973).
66. Horner, M. A., Fleming, T. H. & Sahey, C. T. Foraging behaviour and energetics of a nectar-feeding bat, *Leptonycteris curasoae* (Chiroptera: Phyllostomidae). *J. Zool.* **244**, 575–586 (1998).

67. Huttlin, E. L. et al. A tissue-specific atlas of mouse protein phosphorylation and expression. *Cell* **143**, 1174–1189 (2010).
68. Freitas, M. B. et al. Reduced insulin secretion and glucose intolerance are involved in the fasting susceptibility of common vampire bats. *Gen. Comp. Endocrinol.* **183**, 1–6 (2013).
69. Simpson, I. A. et al. The facilitative glucose transporter GLUT3: 20 years of distinction. *Am. J. Physiol.-Endocrinol. Metab.* **295**, E242–E253 (2008).
70. Hutcheon, J. M., Kirsch, J. A. & Garland, T. Jr A comparative analysis of brain size in relation to foraging ecology and phylogeny in the Chiroptera. *Brain. Behav. Evol.* **60**, 165–180 (2002).
71. Hall, R. P. et al. Find the food first: an omnivorous sensory morphotype predates biomechanical specialization for plant based diets in phyllostomid bats. *Evolution* **75**, 2791–2801 (2021).
72. Amaral, T. S., Pinheiro, E. C., Freitas, M. B. & Aguiar, L. M. S. Low energy reserves are associated with fasting susceptibility in Neotropical nectar bats *Glossophaga soricina*. *Braz. J. Biol.* **79**, 165–168 (2018).
73. Potter, J. H. T. et al. Dietary diversification and specialization in neotropical bats facilitated by early molecular evolution. *Mol. Biol. Evol.* **38**, 3864–3883 (2021).
74. Fisher, R. B. & Parsons, D. S. The gradient of mucosal surface area in the small intestine of the rat. *J. Anat.* **84**, 272–282 (1950).
75. Riesenfeld, G., Sklan, D., Bar, A., Eisner, U. & Hurwitz, S. Glucose absorption and starch digestion in the intestine of the chicken. *J. Nutr.* **110**, 117–121 (1980).
76. Wright, E. M., Sala-Rabanal, M., Ghezzi, C. & Loo, D. D. F. in *Physiology of the Gastrointestinal Tract*, 6th edn (ed. Said, H. M.) 1051–1062 (Elsevier, 2018).
77. Silva, C. et al. Comparative study on the small and large intestines of the bats *Artibeus planirostris* and *Diphylla ecaudata*: influence of food habits on morphological parameters. *Acta Chiropterologica* **22**, 435–448 (2020).
78. Park, H. & Hall, R. The gross anatomy of the tongues and stomachs of eight new world bats. *Trans. Kans. Acad. Sci.* **54**, 64–72 (1951).
79. Nicolson, S. W. Sweet solutions: nectar chemistry and quality. *Philos. Trans. R. Soc. B* **377**, 20210163 (2022).
80. Göttlinger, T., Schwerdtfeger, M., Tiedge, K. & Lohaus, G. What do nectarivorous bats like? Nectar composition in Bromeliaceae with special emphasis on bat-pollinated species. *Front. Plant Sci.* **10**, 205 (2019).
81. Hilton, W. A. The morphology and development of intestinal folds and villi in vertebrates. *Am. J. Anat.* **1**, 459–505 (1902).
82. Walton, K. D., Mishkind, D., Riddle, M. R., Tabin, C. J. & Gumucio, D. L. Blueprint for an intestinal villus: species-specific assembly required. *Wiley Interdiscip. Rev. Dev. Biol.* **7**, e317 (2018).
83. Strobel, S., Encarnação, J. A., Becker, N. I. & Trenczek, T. E. Histological and histochemical analysis of the gastrointestinal tract of the common pipistrelle bat (*Pipistrellus pipistrellus*). *Eur. J. Histochem.* **59**, 2477 (2015).
84. Scillitani, G., Zizza, S., Liquori, G. E. & Ferri, D. Lectin histochemistry of gastrointestinal glycoconjugates in the greater horseshoe bat, *Rhinolophus ferrumequinum* (Schreber, 1774). *Acta Histochem.* **109**, 347–357 (2007).
85. Gadelha-Alves, R., Rozensztranch, A. M. D. S. & Rocha-Barbosa, O. Comparative intestinal histomorphology of five species of phyllostomid bats (Phyllostomidae, Microchiroptera): ecomorphological relations with alimentary habits. *Int. J. Morphol.* **26**, 591–602 (2008).
86. Novaes, R. L. M. et al. First evidence of frugivory in Myotis (Chiroptera, Vespertilionidae, Myotinae). *Biodivers. Data J.* https://doi.org/10.3897/BDJ.3.e6841 (2015).
87. Makanya, A., John, M., Mayhew, T., Tschanz, S. & Burri, P. A stereological comparison of villous and microvillous surfaces in small intestines of frugivorous and entomophagous bats: species, inter-individual and craniocaudal differences. *J. Exp. Biol.* **200**, 2415–2423 (1997).
88. Makanya, A. N., Self, T. J., Warui, C. N. & Mwangi, D. K. Gut morphology and morphometry in the epauletted wahlbergs fruit bat (*Epomophorus wahlbergi*, Sundevall, 1846). *Acta Biol. Hung.* **52**, 75–89 (2005).
89. Caviedes-Vidal, E. et al. Paracellular absorption: a bat breaks the mammal paradigm. *PLoS ONE* **3**, e1425 (2008).
90. Brun, A. et al. High paracellular nutrient absorption in intact bats is associated with high paracellular permeability in perfused intestinal segments. *J. Exp. Biol.* **217**, 3311–3317 (2014).
91. Brun, A. et al. Morphological bases for intestinal paracellular absorption in bats and rodents. *J. Morphol.* **280**, 1359–1369 (2019).
92. Fasulo, S. V. Absorción intestinal en mamíferos. Evaluación comparativa de la ruta paracelular en mamíferos terrestres y voladores. *Mastozool. Neotropical* **21**, 180–181 (2014).
93. Price, E. R., Brun, A., Caviedes-Vidal, E. & Karasov, W. H. Digestive adaptations of aerial lifestyles. *Physiology* **30**, 69–78 (2015).
94. Shirazi-Beechey, S. P., Moran, A. W., Batchelor, D. J., Daly, K. & Al-Rammahi, M. Glucose sensing and signalling; regulation of intestinal glucose transport. *Proc. Nutr. Soc.* **70**, 185–193 (2011).
95. Ali, R. S. et al. Glucose transporter expression and regulation following a fast in the ruby-throated hummingbird, *Archilochus colubris*. *J. Exp. Biol.* **223**, jeb229989 (2020).
96. Meng, F., Zhu, L., Huang, W., Irwin, D. M. & Zhang, S. Bats: body mass index, forearm mass index, blood glucose levels and SLC2A2 genes for diabetes. *Sci Rep.* **6**, 29960 (2016).
97. Pinheiro, E. C., Taddei, V. A., Migliorini, R. H. & Kettelhut, I. C. Effect of fasting on carbohydrate metabolism in frugivorous bats (*Artibeus lituratus* and *Artibeus jamaicensis*). *Comp. Biochem. Physiol. B* **143**, 279–284 (2006).
98. Tobin, V. et al. Insulin internalizes GLUT2 in the enterocytes of healthy but not insulin-resistant mice. *Diabetes* **57**, 555–562 (2008).
99. Suarez, R. K. & Welch, K. C. Sugar metabolism in hummingbirds and nectar bats. *Nutrients* **9**, 743 (2017).
100. Voigt, C. C. & Speakman, J. R. Nectar-feeding bats fuel their high metabolism directly with exogenous carbohydrates. *Funct. Ecol.* **21**, 913–921 (2007).
101. Marks, J., Carvou, N. J. C., Debnam, E. S., Srai, S. K. & Unwin, R. J. Diabetes increases facilitative glucose uptake and GLUT2 expression at the rat proximal tubule brush border membrane. *J. Physiol.* **553**, 137–145 (2003).
102. Ait-Omar, A. et al. GLUT2 accumulation in enterocyte apical and intracellular membranes. *Diabetes* **60**, 2598–2607 (2011).
103. Gromova, L. V., Fetissov, S. O. & Gruzdkov, A. A. Mechanisms of glucose absorption in the small intestine in health and metabolic diseases and their role in appetite regulation. *Nutrients* **13**, 2474 (2021).
104. Freeman, P. W. in *Bat Biology and Conservation* (eds Kunz T. H. & Racey, P. A.) 140–156 (Smithsonian Institution Scholarly Press, 1998).
105. Rojas, D., Vale, A., Ferrero, V. & Navarro, L. When did plants become important to leaf-nosed bats? Diversification of feeding habits in the family Phyllostomidae. *Mol. Ecol.* **20**, 2217–2228 (2011).
106. Santana, S. E., Strait, S. & Dumont, E. R. The better to eat you with: functional correlates of tooth structure in bats. *Funct. Ecol.* **25**, 839–847 (2011).
107. Kurta, A., Bell, G. P., Nagy, K. A. & Kunz, T. H. Energetics of pregnancy and lactation in freeranging little brown bats (*Myotis lucifugus*). *Physiol. Zool.* **62**, 804–818 (1989).
108. Voigt, C. Reproductive energetics of the nectar-feeding bat *Glossophaga soricina* (Phyllostomidae). *J. Comp. Physiol. B* **173**, 79–85 (2003).

109. Bürkner, P. C. Advanced Bayesian multilevel modeling with the R package brms. *R J.* **10**, 395–411 (2018).
110. Paradis, E. & Schliep, K. ape 5.0: an environment for modern phylogenetics and evolutionary analyses in R. *Bioinformatics* **35**, 526–528 (2018).
111. Revell, L. J. phytools: An R package for phylogenetic comparative biology (and other things). *Methods Ecol. Evol.* **3**, 217–223 (2012).
112. R Core Team. *R: A Language and Environment for Statistical Computing* (R Foundation for Statistical Computing, 2023).
113. Schindelin, J. et al. Fiji: an open-source platform for biological-image analysis. *Nat. Methods* **9**, 676–682 (2012).
114. Ishida, M. et al. The comparative anatomy of the folds, fossae, and adhesions around the duodenojejunal flexure in mammals. *Folia Morphol.* **77**, 286–292 (2018).
115. consortium, U. UniProt: the universal protein knowledgebase in 2021. *Nucleic Acids Res.* **49**, D480–D489 (2020).
116. Buels, R. et al. JBrowse: a dynamic web platform for genome visualization and analysis. *Genome Biol.* **17**, 66 (2016).
117. Spoor, S. et al. Tripal v3: an ontology-based toolkit for construction of FAIR biological community databases. *Database* **2019**, baz077 (2019).
118. Capella-Gutiérrez, S., Silla-Martínez, J. M. & Gabaldón, T. trimAl: a tool for automated alignment trimming in large-scale phylogenetic analyses. *Bioinformatics* **25**, 1972–1973 (2009).
119. Dylus, D. et al. How to build phylogenetic species trees with OMA. *F1000Research* **9**, 511 (2022).
120. Miller-Butterworth, C. M. et al. A family matter: conclusive resolution of the taxonomic position of the long-fingered bats, miniopterus. *Mol. Biol. Evol.* **24**, 1553–1561 (2007).
121. Lim, B. Review of the origins and biogeography of bats in South America. *Chiropt. Neotrop.* **15**, 391–410 (2009).
122. Rojas, D., Warsi, O. & Davalos, L. Bats (Chiroptera: Noctilionoidea) challenge a recent origin of extant neotropical diversity. *Syst. Biol.* **65**, 432–448 (2016).
123. Livak, K. J. & Schmittgen, T. D. Analysis of relative gene expression data using real-time quantitative PCR and the $2^{-\Delta\Delta CT}$ method. *Methods* **25**, 402–408 (2001).

Acknowledgements

A portion of the fieldwork was carried out within the framework of the project 'Contribución a la conservación del Bosque seco Tropical del Valle del Cauca' under the CVC permit no. 1122 of 2018, from the Institute for Research and Preservation of the Cultural and Natural Heritage of Valle del Cauca, whom we thank, along with the support of J.O. Ortíz, R. Rivera and A.Bernal and the field assistance from Therios (Cali, Colombia), C. Calvache, S. Tabares, A. Chito and O. Cuellar. Thanks to M. Eifler at the KU Biodiversity Institute and Natural History Museum, N. Simmons and M. Surovy from the AMNH for facilitating access and research of museum specimens. We thank the scientists at the Stowers Institute for Medical Research, S. Malloy, H. Wilson, M. Frangello, C. Maddera and X. Zhao, for help in processing and imaging histological and electron microscopy sections, as well as D. Bradford for providing training on RT–qPCR instrumentation and data analysis. We also thank J. A. Riascos for the bat illustration in the graphical abstract; D. Narang, R. Smith and S. Mahadeo for their support in Trinidad; F. Reid and J. Jamison for their support in Costa Rica; S. Sanatana for guidance in phylogenetic comparative methods analysis; and A. Sadier and L. Yohe for comments that improved this manuscript. Finally, we thank the Rohner lab members for creating a stimulating scientific environment and for their support during the manuscript writing. Funding for the project was provided by the Stowers Institute and National Institutes of Health (NIH) grant no. 1DP2AG071466-01 to N.R., the National Science Foundation (NSF) Postdoctoral Research Fellowships in Biology no. 2109717 (2021–2022) to J.C., the Burroughs Wellcome Fund (BWF) Postdoctoral Diversity Enrichment Program (G-1022339) to J.C. and the Howard Hughes Medical Institute (HHMI) Hanna H. Gray Fellows Program (GT15991) to J.C. Any opinions, findings and conclusions or recommendations expressed in this material are those of the authors and do not necessarily reflect the views of the NIH, NSF, BWF or HHMI.

Author contributions

A.B.-R. and J.C. designed the study. A.B.-R., J.C. and V.P. designed the figures. A.B.-R. performed the in vivo physiology experiments as an undergraduate thesis project (2019–2020) directed by O.E.M.-G. A.B.-R. and O.E.M.-G. designed the in vivo physiology experiments and performed the statistical analyses. A.B.-R. and J.C. performed additional glucose tolerance tests and obtained gut tissue for molecular analyses in April 2022. A.B.-R. and J.C. dissected the gastrointestinal tract of museum bats and performed morphological data interpretation. K.Y. performed the TEM experiments and imaging. A.B.-R. made the gut anatomy measurements and comparisons. S.M.C.R. produced gene models across the assembled genomes, assigned orthologs, built webpages and genome browsers and generated the phylogenomic tree. J.R. and J.C. performed selection tests. J.R. performed Alphafold and Foldseek analysis. J.C., D.T. and Y.W. performed the HCR experiments, J.C. and V.P. performed HCR imaging, and J.C. performed HCR analysis. V.P. and P.M.-S. extracted RNA from the duodenum, and P.M.-S. performed qPCR. A.B.-R., J.C. and N.R. co-wrote the manuscript.

Competing interests

The authors declare no competing interests.

Additional information

Extended data is available for this paper at https://doi.org/10.1038/s41559-024-02485-7.

Supplementary information The online version contains supplementary material available at https://doi.org/10.1038/s41559-024-02485-7.

Correspondence and requests for materials should be addressed to Jasmin Camacho, Oscar E. Murillo-García or Nicolas Rohner.

Peer review information *Nature Ecology & Evolution* thanks Zixia Huang, Ekaterina Osipova and the other, anonymous, reviewer(s) for their contribution to the peer review of this work. Peer reviewer reports are available.

https://doi.org/10.1038/s41559-024-02485-7

A

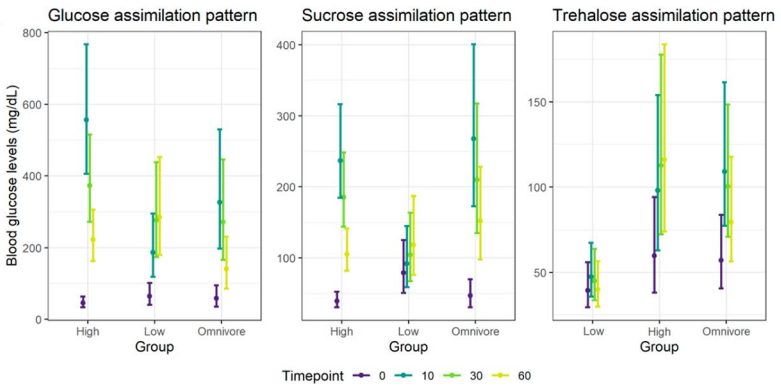

B

Phylogenetic signal			
Sugar	**Variable**	**Lambda (λ)**	**P-value**
Glucose	Assimilation proxy	0.988169	0.0584431
Sucrose	Assimilation proxy	**0.999927**	**0.0158425**
Trehalose	Assimilation proxy	**0.70459**	**0.281583**

Extended Data Fig. 1 | Phylogenetic signal. a) Comparison of assimilation curves for glucose, sucrose, and trehalose solutions among Neotropical bats with different food preferences: high sugar in glucose and sucrose graphs refer to frugivorous and nectarivorous bats, while low sugar refers to insectivorous, carnivorous and hematophagous bats; high sugar in the trehalose graph refers to insectivorous bats and low sugar refers to the rest of the dietary categories; omnivores have their own category because they have diets where the three sugars are present in relatively high proportions. The Bayesian multilevel phylogenetic model estimated blood glucose levels for each time point and for each group, data are presented as mean values +/− SEM; we included the taxa for which we had data for each individual sugar (Supplemental Table 1). For glucose assimilation we included 22 species, for sucrose assimilation 18 species and for trehalose assimilation 19 species. **b**) Table. Phylogenetic signal (Pagel's λ) evaluated for the assimilation proxy (corrected area under the curve) of glucose, sucrose and trehalose in Neotropical bats.

https://doi.org/10.1038/s41559-024-02485-7

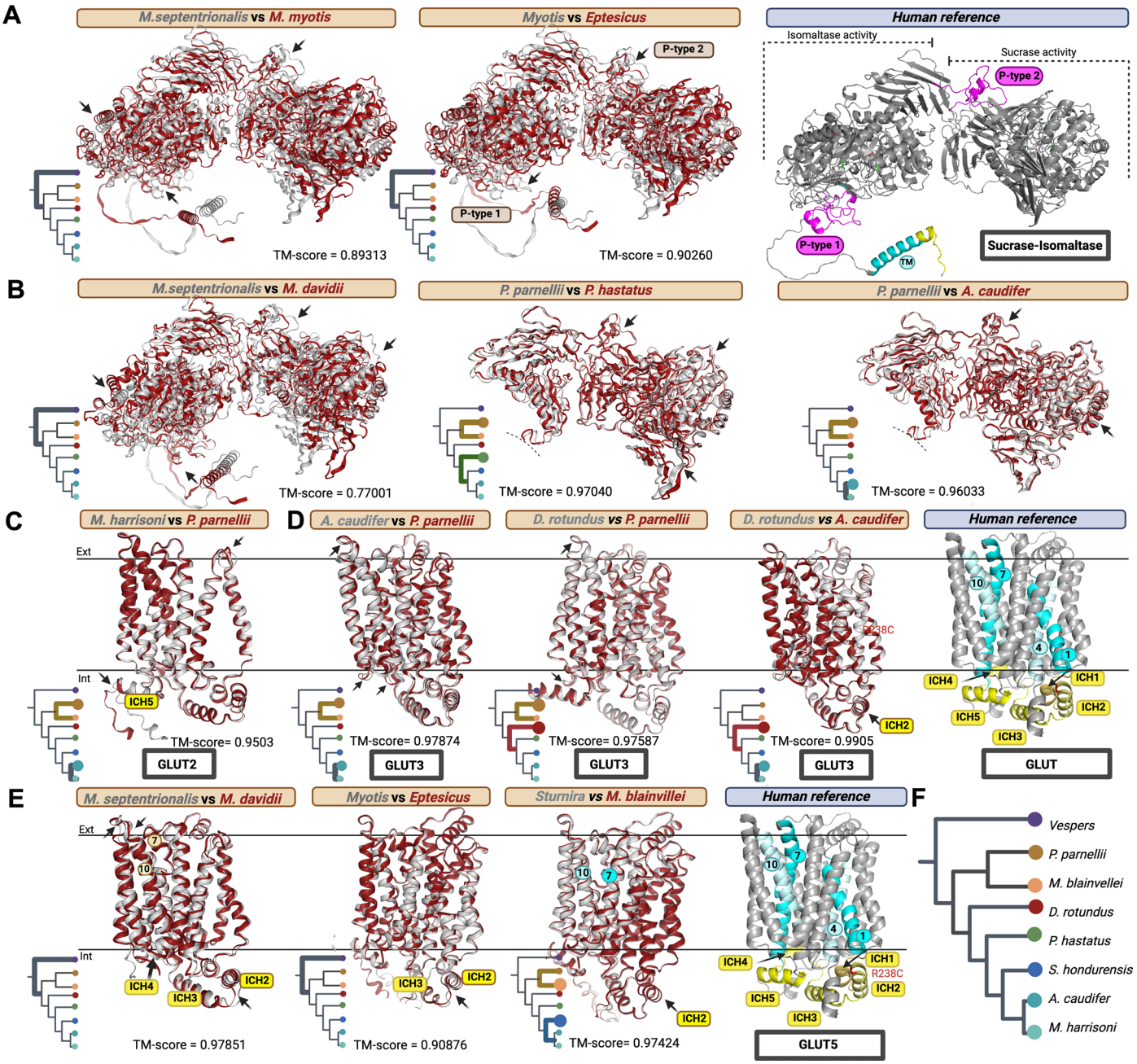

Extended Data Fig. 2 | See next page for caption.

https://doi.org/10.1038/s41559-024-02485-7

Extended Data Fig. 2 | Alphafold protein predictions and foldseek comparisons. Ribbon representation of AlphaFold modeled proteins, viewed in the plane of the membrane, from positive selected genes. The human reference protein structure has functional protein features highlighted using PyMOL for protein orientation as follows for 1) SI: P-type 1 and 2 are colored in magenta, the binding sites for sugar are colored in green, and the known mutations that affect function are colored in red (**a-b**); and 2) GLUTs: transmembrane (TM) 1 and 4 in the N-terminal domain are colored in cyan and light cyan, respectively; TM 7 and 10 in the C-terminal bundle are colored in cyan and light cyan, respectively; intracellular domain helices (ICH) unique to the sugar transporters are shown in yellow (**c-e**); single amino acid change (R238C) in the human GLUT5 model relates to colon cancer (Warburg effect, Tate et al. 2019). For each GLUT transporter shown, the C-terminal transmembrane (TM) bundle is located on the left and the N-terminal TM bundle is located on the right. The C- and N- terminal TM bundles transport glucose with a rocker-switch-type movement1. TM7 and TM10 support a gated-pore mechanism for glucose binding and release. The intracellular helices (ICH) domain provides stabilization for conformational changes. Foldseek structural comparisons between pairs of species for **a-b**) SI; **c**) GLUT2; **d**) GLUT3; and **e**) GLUT5. Each protein comparison is based on genes undergoing positive selection and is phylogenetically informed (**f**). Observed structural changes are summarized as a TM-score (TM-score = 1 is a perfect structural match). Arrows highlight structural changes in SI that relate to enzymatic function and in GLUTs where glucose binds extracellularly (ext) and where structural changes might affect substrate transport (int). (**a**) Folkseek comparisons for sucrase-isomaltase (SI) of vesper bats in the genus *Myotis* and *Eptesicus*. We observe global differences among *Mytois* species in the sucrase subunit's P-type 2 domain, as well as the isomaltase subunit P-type 1 domain. SI activity relies on attachment to the gastrointestinal mucosa's plasma membrane, facilitated by the isomaltase subunit's P-type 1 domain. Further, changes along the alpha and beta strands of both subunits have been known to cause dissociation of SI from the membrane and a single amino acid change in the second helical domain of the isomaltase subunit is sufficient to cause dissociation of SI from the membrane and the inability to process sucrose. It is possible that the changes in *Myotis*, compared to other insect-feeding bats like *Eptesicus*, provides the ability to process sugar, preventing them from having intestinal malabsorption and intestinal distress from undigested sugar. Greater differences in *Myotis* SI structure may reflect their ability to assimilate sucrose. (**b**) Folkseek comparisons for SI structure for *Myotis, P. parnellii, P. hastatus,* and *A. caudifer*. For the sugar-eating phyllostomid bats, we observe localized changes to the isomaltase subunit's P-type 1 domain, which is in line with the fact that ingesting high-sugar sources is expected to increase sugar metabolism proteins, particularly *SI* expression. (**c**) We detected positive selection in *Slc2a2* in the ancestral branch leading to nectarivores as well as in *M. harrisonii*. Compared to the outgroup species *P. parnellii*, we observe differences predicted to be along the extracellular N-terminal between TM bundles 4 and 5, which is usually highly conserved among sugar transporters. We also predicted differences along the C-terminal end of the ICH5 domain, which undergoes post-translational modification for stability along the cell surface of pancreatic beta cells. **d**) GLUT3 predicted structure and Foldseek comparisons between nectar bat *A. caudifer* (gray) and *P. parnellii* (red); vampire bat *D. rotundus* (gray) and *P. parnellii* (red), and *D. rotundus* (gray) and *A. caudifer* (red). The amino acid substitutions are located along extracellular C-terminal transmembrane (TM) 10, where glucose binds, as well as within the plasma membrane, where it interacts with TM7 to coordinate glucose transport. We also identified changes at the intracellular side of the C-terminal domain, possibly affecting the degree of opening during glucose transport. This implies that the GLUT3 transporter may undergo modifications to glucose delivery to the brain's neurons that may contribute to protection against their heightened susceptibility to fasting. **e**) Folkseek comparisons for GLUT5 predictions between *Myotis* species, the genus *Myotis* (gray) and *Eptesicus* (red), and the fruit bat *S. hondurensis* (gray) and insect bat *M. blainvillei* (red). We observe differences along the intracellular helices (ICH) domain 2-3, which anchor the conformational changes needed to transport glucose/fructose.

https://doi.org/10.1038/s41559-024-02485-7

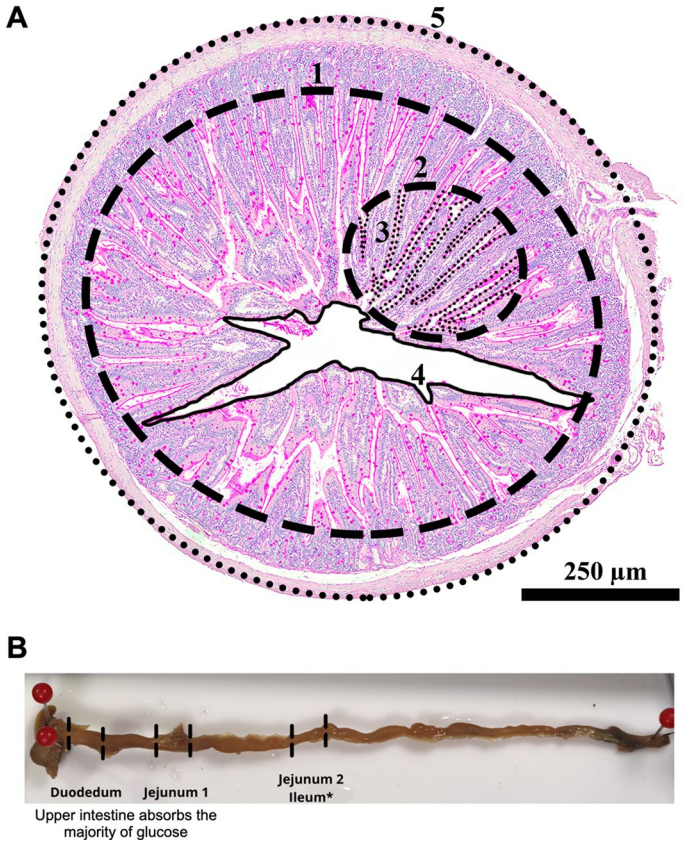

Extended Data Fig. 3 | Measurements from museum samples. a) Measures extracted from the intestine cross sections. 1. Villi-lumen area (VLA); 2. Sample area (SA); 3. Villi perimeter in the sampled area (VPSA); 4. Lumen area (LA); 5. Cross section perimeter (CSP). The measurements for the VPSA were taken twice with similar results. **b**) Intestinal segments selected for analysis. The duodenum is the first section of the intestine from the end of the stomach-pylorus to the duodenojejunal flexure. The jejunum is the next proximal ~2/3 of the small intestine until the presence of peyer's patches, which marks the ileum, through histology.

https://doi.org/10.1038/s41559-024-02485-7

A

	Fragment length bp	5' - 3' primer sequence	Primer origin
Gapdh	137	F: CCT TCA TTG ACC TCA ACT AC R: ATC TCG CTC CTG GAA GAT	This study
Slc2a2	120	F: CCG ACA GCC TAT TCT AGT GGC ATT G R: TGT TGA TGG CAC CAA CTC CGA TG	This study
Sglt1	100	F: GTT GGA TTC TTC CTG R: CCA GCC CCA CAA AGT	This study
SI	126	F: CTG GAT CCA GCA ATT TCA R: ATC TGG CCA AAC CTT TG	This study

B

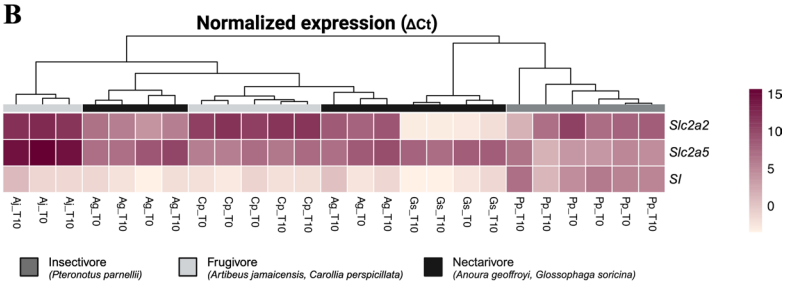

C

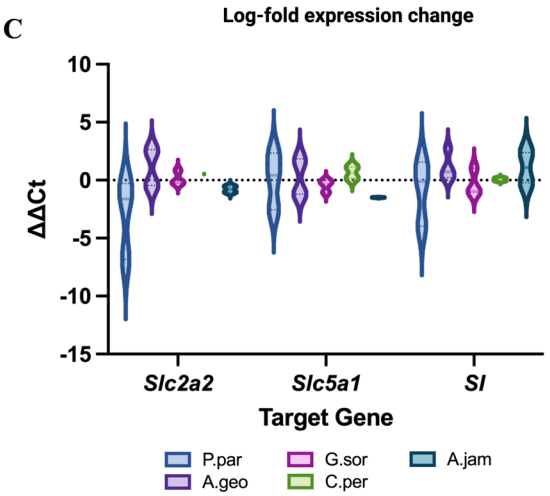

D

		Sum of squares	DF	Mean square	F	P-value
Slc2a2	Treatment	30.09	4	7.52	F (4,9) = 1.999	p = 0.178
	Residuals	33.87	9	3.76		
	Total	63.97	13			
Sglt1	Treatment	5.95	4	1.49	F (4,9) = 0.615	p = 0.663
	Residuals	21.76	9	2.42		
	Total	27.71	13			
SI	Treatment	8.666	4	2.167	F (4,9) = 0.743	p = 0.5862
	Residuals	26.24	9	2.916		
	Total	34.91	13			

Extended Data Fig. 4 | qPCR summary. (**a**) Primer sequences. (**b**) RT-qPCR heatmap of normalized expression (ΔCt) relative to housekeeping gene *Gapdh* for nutrient transporter genes *Slc2a2*, *Slc5a1* and digestive enzyme gene *SI*. Five species representing four dietary guilds are shown [insect, *Ptenonotus parnellii* (Pp, nt=10 = 3, nt=0 = 3); omnivore, *Carollia perspicillata* (Cp, nt=10 = 2, nt=0 = 3); fruit, *Artibeus jamaicensis* (Aj, nt=10 = 2, nt=0 = 1); nectar, *Anoura geoffroyi* (Ag, nt=10 = 4, nt=0 = 3) and *Glossophaga soricina* (Gs, nt=10 = 3, nt=0 = 1)]. Samples are ordered by hierarchical clustering using Euclidean distance and the colors assigned to the clusters correspond to the dietary guild. (**c**) Logfold expression change (ΔΔCt) of *Slc2a2*, *Slc5a1* and *SI* at t = 10 relative to t = 0. (**d**) No significant differences in logfold expression change were determined between t = 10 and t = 0 individuals for species by one-way ANOVA (*Slc2a2*; p = 0.178, *Slc5a1*; p = 0.663, *SI*; p = .0568).

https://doi.org/10.1038/s41559-024-02485-7

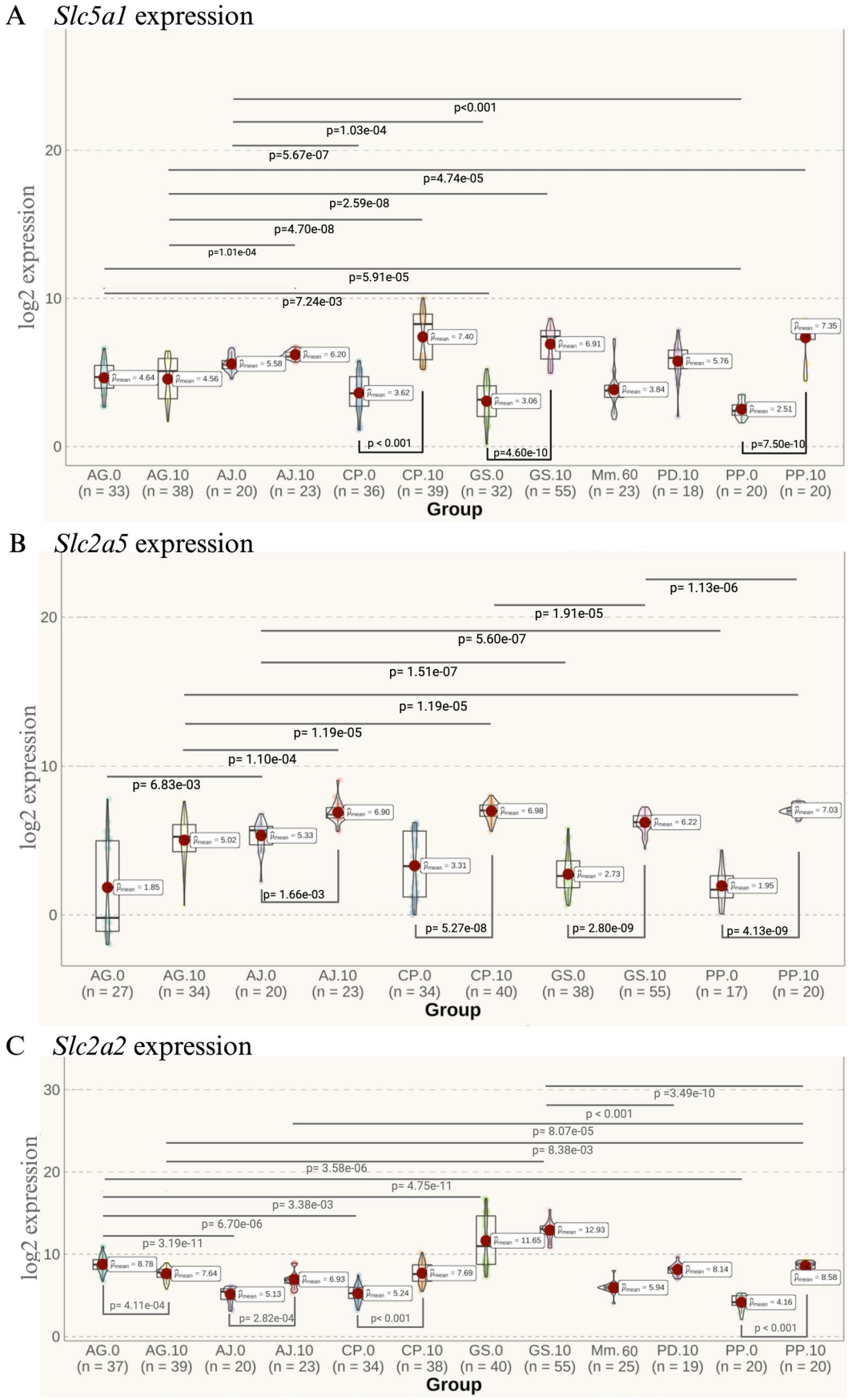

Extended Data Fig. 5 | See next page for caption.

https://doi.org/10.1038/s41559-024-02485-7

Extended Data Fig. 5 | HCR data. HCR RNA-FISH data for *Slc5a1* (**A**), *Slc2a5* (**B**), and *Slc2a2* (**C**). Image data for fluorescence intensity was log2 transformed for comparisons between time points within a species and across species. Two to three sections per individual with good morphology were chosen for study. For each section, 5-10 cells were isolated for analysis. Fluorescence signals were quantified using threshold-based segmentation and spot detection (n = 17-55 cells per treatment per species) in FIJI. We performed Games-Howell pairwise comparisons using the ggstatsplot function in R, with holm-bonferroni p-adjustments for multiple comparisons. Within each boxplot, a red dot denotes mean values, horizontal black lines denote median values, the boxes represent the range from the 25th to the 75th percentile of each group's value distribution, while the vertical lines indicate the most extreme values within 1.5 times the interquartile range from the 25th and 75th percentiles of each group. Mean values are listed in Extended Data Table 5. Comparisons within species (t = 0 vs. t = 10) with significant expression level differences are bracketed at the bottom of each boxplot graph as follows: AGt0-t10 *Slc2a2* (padj=4.11e-04), AJt0-t10 *Slc2a5* (padj=1.66e-03), AJt0-t10 *Slc2a2* (padj=2.82e-04), CPt0-t10 *Slc5a1* (padj=0.0001), CPt0-t10 *Slc2a5* (padj=5.27e-08), CPt0-t10 *Slc2a2* (padj=0.001), GSt0-t10 *Slc5a1* (padj=4.60e-10), GSt0-t10 *Slc2a5* (padj=2.80e-09), PPt0-t10 *Slc5a1* (padj=7.50e-10), PPt0-t10 *Slc2a5* (padj=4.13e-09), PPt0-t10 *Slc2a2* (padj=0.001).Comparisons between species at each respective time point are shown at the top of each graph, where only significant data (padj < 0.001) are shown as follows: *Slc5a1* (A) AGt0-GSt0 (padj=7.24e-03), AGt0-PPt0 (padj=5.91e-05), AJt0-GSt0 (padj=1.03e-03), AJt0-PPt0 (padj=0.001), AJt0-CPt0 (padj=5.67e-07), AGt10-AJt10 (padj=1.01e-04), AGt10-CPt10 (padj=4.70e-08), AGt10-GSt10 (padj=2.59e-08). AGt10-CPt10 (padj=4.74e-05); *Slc2a5* (B) AGt0-AJt0 (padj=6.83e-03), AJt0-PPt0 (padj=5.60e-07), AGt10-AJt10 (padj=1.10e-04), AGt10-CPt10 (padj=1.19e-05), AGt10-PPt10 (padj=1.19e-05), CPt10-GSt10 (padj=1.91e-05), GSt10-PPt10 (padj=1.13e-06); *Slc2a2* (C) AGt0-GSt0 (padj=3.38e-03), AGt0-PPt0 (p = 4.75e-11), AGt0-AJt0 (padj=3.19e-11), AGt0-CPt0 (padj=6.70e-06), AGt10-GSt10 (padj=3.58e-06), AGt10-PPt10 (padj=8.38e-03), GSt10-PDt10 (padj=0.001), AJt10-PPt10 (padj=8.07e-05), GSt10-PPt10 (padj=3.49e-10). The following species represent each dietary guild: insects, *Ptenonotus parnellii* (PP, n = 4) and *Micronycteris minuta* (Mm n = 1); omnivore, *Carollia perspicillata* (CP, n = 4); fruit, *Artibeus jamaicensis* (AJ, n = 2); nectar, *Glossophaga soricina* (GS, n = 4) and *Anoura geoffroyi* (AG, n = 4). *Phyllostomus discolor* (PD, n = 1), is an omnivorous bat that has a large portion of nectar in their diet. Only technical replicates are available for species with n = 1.

https://doi.org/10.1038/s41559-024-02485-7

Extended Data Table 1 | Glucose tolerance test with different sugars

Family	Genus	Food preference	Sugar	# Individuals	Species
Phyllostomidae	*Artibeus*	Fruits	Trehalose	17	*A. lit, A. pla, A. aeq*
			Sucrose	22	
			Glucose	13	
	Dermanura		Trehalose	6	*D. pha*
			Sucrose	6	
			Glucose	6	
	Uroderma		Trehalose	1	*U. con, U. bak*
			Sucrose	1	
			Glucose	1	
	Platyrrhinus		Sucrose	1	*P. hel*
	Sturnira		Trehalose	1	*S. gia, S. lud, S. lui, S. par*
			Sucrose	1	
			Glucose	3	
	Glossophaga	Nectar	Trehalose	4	*G. sp.*
			Sucrose	6	
			Glucose	4	
	Choeroniscus		Trehalose	1	*C. god*
			Sucrose	1	
			Glucose	2	
	Lonchophylla		Glucose	5	*L. con, L. rob*
	Carollia	Fruits & Insects	Trehalose	18	*C. cas, C. per, C. bre*
			Sucrose	19	
			Glucose	13	
	Phyllostomus	Insects, Nectar, Polen, Fruits, Vertebrates	Trehalose	3	*P. dis, P. has*
			Sucrose	1	
			Glucose	1	
	Vampyrum	Vertebrates	Glucose	1	*V. spe*
	Desmodus	Blood	Trehalose	4	*D.rot*
			Sucrose	4	
			Glucose	6	
	Gardnerycteris	Insects	Trehalose	1	*G. cre*
Mormoopidae	*Pteronotus*		Glucose	12	*P. par*
Vespertilionidae	*Myotis*		Trehalose	3	*M. cau, M. alb*
			Sucrose	1	
			Glucose	2	
Molossidae	*Molossus*		Trehalose	1	*M. mol*
			Glucose	1	
Emballonuridae	*Saccopteryx*		Trehalose	1	*S. bil*
			Sucrose	1	
			Glucose	1	
	Peropteryx		Sucrose	3	*P. kap*
Total				**199**	**29**

Species included in the in vivo physiology essay. *A. lit: Artibeus lituratus, A. pla: Artibeus planirostris, A. aeq: Artibeus aequatorialis, D. pha: Dermanura phaeotis, U. con: Uroderma convexum, U. bak: Uroderma bakeri, P. hel: Platyrrhinus helleri, S. gia: Sturnira giannae, S. lud: Sturnira ludovici, S. lui: Sturnira luisi, S. par: Sturnira parvidens, G. sp.: Glossophaga sp., C. god: Choeroniscu godmani, L. con: Lonchophylla concava, L. rob: Lonchophylla robusta, C. cas: carollia castanea, C. per: Carollia perspicillata, C. bre: Carollia brevicauda, P. dis: Phyllostomus discolor, P. has: Phyllostomus hastatus, V. spe: Vampyrum spectrum, D. rot: Desmodus rotundus, G. cre: Gardnerycteris crenulatum, M. cau: Myotis caucensis, M. alb: Myotis albescens, M. mol: Molossus molossus, S. bil: Saccopteryx billineata, P. kap: Peropteryx kappleri.*

https://doi.org/10.1038/s41559-024-02485-7

Extended Data Table 2 | Bat genomes

A. Bat genomes used for positive selection tests

Family	Species	Year published	NCBI accession	RNAseq/ Proteome	Species Code
Vespertilionidae	*Eptesicus fuscus*	2020	*DNAzoo SRS7189612	GCF_000308155.1	EFU
Vespertilionidae	*Myotis myotis*	2020	GCA_014108235.1	GCF_014108235.1	MMY
Vespertilionidae	*Myotis septentrionalis*	2020	*DNAzoo SRS7189622	Hi-C	MSE
Molossidae	*Molossus molossus*	2020	GCA_014108415.1	GCF_014108415.1, SRR9703456	MMO
Miniopteridae	*Miniopterus natalensis*	2016	GCA_001595765.1	GCF_001595765.1	MNA
Miniopteridae	*Miniopterus schreibersii*	2019	GCA_004026525.1	n/a	MSC
Mormoopidae	*Pteronotus parnellii*	2013	GCA_000465405.1	SRR9703452, PRJNA481095, PRJNA481095	PPA
Mormoopidae	*Mormoops blainvillei*	2019	GCA_004026545.1	SRR9703451	MBL
Phyllostomidae	*Desmodus rotundus*	2018	GCA_002940915.1	GCF_002940915.1, SRR9703482, PRJNA178123, SRR8878915	DRO
Phyllostomidae	*Anoura caudifer*	2019	GCA_004027475.1	SRR9703485	ACA
Phyllostomidae	*Musonycteris harrisonii*	2021	*Gigadb 100746	n/a	MHA
Phyllostomidae	*Leptonycteris nivalis*	2020	PRJNA543656	n/a	LNI
Phyllostomidae	*Leptonycteris yerbabuenae*	2020	PRJNA627035	SRR9087861, SRR9087862, SRR9087863, SRR9087864	LYE
Phyllostomidae	*Macrotus waterhousii*	2020	*Gigadb 100746	SRR9703483	MWA
Phyllostomidae	*Macrotus californicus*	2019	GCA_007922815.1	n/a	MCA
Phyllostomidae	*Micronycteris hirsuta*	2019	GCA_004026765.1	n/a	MHI
Phyllostomidae	*Tonatia saurophila*	2019	GCA_004024845.1	n/a	TSA
Phyllostomidae	*Phyllostomus discolor*	2019	GCA_004126475.2	GCF_004126475.2	PDI

A. Bat genomes used for positive selection tests (continued)

Family	Species	Year published	NCBI accession	RNAseq/ Proteome	Species Code
Phyllostomidae	*Phyllostomus hastatus*	2021	GCA_019186645.1	SRR9703480	PHA
Phyllostomidae	*Sturnira hondurensis*	2020	GCA_014824575.2	GCF_014824575.2	SHO
Phyllostomidae	*Carollia perspicillata*	2019	GCA_004027735.1	SRR9703464, SRR5872538	CPE
Phyllostomidae	*Artibeus jamaicensis*	2019	GCA_004027435.1	SRR9703479, SRR539297, PRJNA305413	AJA
Primates	*Homo sapiens*	2019	GCA_000001405.28	GCF_000001405.39	HSA
Eulipotyphla	*Sorex araneus*	2012	GCA_000181275.2	n/a	SAR

B. Additional bat genomes used for protein predictions

Family	Species	Year published	NCBI accession		Species Code
Vespertilionidae	*Myotis brandtii*	2013	GCF_000412655.1		MYB
Vespertilionidae	*Myotis davidii*	2012	GCF_000327345.1		MDA
Vespertilionidae	*Murina aurata feae*	2019	GCA_004026665.1		MAU
Molossidae	*Tadarida brasiliensis*	2019	GCA_004025005.1		TBR
Vespertilionidae	*Aeorestes cinereus*	2020	GCA_011751065.1		ACI
Vespertilionidae	*Lasiurus borealis*	2019	GCA_004026805.1		LBO
Vespertilionidae	*Pipistrellus kuhlii*	2020	GCF_014108245.1		PKU
Vespertilionidae	*Pipistrellus pipistrellus*	2020	GCA_903992545.1		PPI
Pteropodidae	*Pteropus alecto*	2013	GCF_000325575.1		PAL
Pteropodidae	*Pteropus rufus*	2020	SRR11097142		PRU
Pteropodidae	*Pteropus alecto*	2013	GCF_000325575.1		PGI
Pteropodidae	*Rousettus aegyptiacus*	2020	GCF_014176215.1		RAE
Pteropodidae	*Rousettus madagascariensis*	2019	SRR11097137		RMA
Pteropodidae	*Eonycteris spelaea*	2018	GCA_003508835.1		ESP
Pteropodidae	*Macroglossus sobrinus*	2019	GCA_004027375.1		MSO
Pteropodidae	*Eidolon helvum*	2013	GCA_000465285.1		EHE
Pteropodidae	*Eidolon dupreanum*	2020	ASM46528v1_HiC		EDU
Hipposideridae	*Hipposideros armiger*	2016	GCF_001890085.1		HAR
Hipposideridae	*Hipposideros galeritus*	2019	GCA_004027415.1		HGA
Rhinolophidae	*Rhinolophus ferrumequinum*	2019	GCA_007922735.1		RFE
Megadermatidae	*Megaderma lyra*	2019	GCA_004026885.1		MLY
Rhinolophidae	*Craseonycteris thonglongyai*	2019	GCA_004027555.1		CTH
Noctilionidae	*Noctilio leporinus*	2019	GCA_004026585.1		NLE

A) Twenty-two bat genomes were assembled and annotated for selection tests. Species were selected to best match the diversity of the in vivo physiology data. Two outgroup genomes, human and shrew, were used to polarize the evolutionary changes in bats. B) In addition to the twenty-two Neotropical bat genomes, we obtained an additional 24 genomes from all available bat species for structural comparisons of proteins with Foldseek.

https://doi.org/10.1038/s41559-024-02485-7

Extended Data Table 3 | Exploratory aBSREL results

A. Statistical summary of the exploratory aBSREL results

Gene	aBSREL Model	AIC_C	logL	Parameters
Slc2a1	Nucleotide GTR	32127.8	-16014.83	49
	Baseline	30189.65	-15002.06	92
	Full adaptive model	29812.02	-14805.1	100
Slc2a2	Nucleotide GTR	74075.49	-36984.67	53
	Baseline	72399.71	-36117.31	82
	Full adaptive model	72101.26	-35951.86	98
Slc2a3	Nucleotide GTR	44911.77	-22402.81	53
	Baseline	43351.46	-21574.92	100
	Full adaptive model	42565.78	-21153.57	128
Slc2a4	Nucleotide GTR	49387.03	-24640.44	53
	Baseline	47689.57	-23744	100
	Full adaptive model	47653.74	-23724.05	102
Slc2a5	Nucleotide GTR	49623.49	-24760.68	51
	Baseline	46931.6	-23379.26	86
	Full adaptive model	46529.65	-23158	106
Slc5a1	Nucleotide GTR	93090.21	-46494.05	51
	Baseline	89484.54	-44653.76	88
	Full adaptive model	88528.46	-44155.46	108
SI	Nucleotide GTR	195876.34	-97887.15	51
	Baseline	191316.64	-95568.12	90
	Full adaptive model	189682.39	-94710.79	130
Treh	Nucleotide GTR	14800.36	-7375.14	25
	Baseline	14468.32	-7185.76	48
	Full adaptive model	14453.92	-7174.49	52

B. Detailed exploratory aBSREL results

Gene	Branch	LRT	p-value	ω distributio
Slc2a1	ACA	170.2147	<0.0001	ω_1= 0.00 (35%) ω_2= 9090 (65%)
	Node 30	13.0492	0.0005	ω_1= 0.00 (99%) ω_2= 111 (0.54%)
Slc2a3	DRO	30.6385	<0.0001	ω_1= 0.104 (98%) ω_2= 247 (1.9%)
	MSE	302.4789	<0.0001	ω_1= 0.00 (46%) ω_2= 868 (54%)
	Node 10	39.5755	<0.0001	ω_1= 0.272 (98%) ω_2= 1e5 (1.7%)
	Node 36	29.7309	<0.0001	ω_1= 0.00 (90%) ω_2=11.6 (9.6%)
	SAR	15.325	0.0002	ω_1= 0. (72%) ω_2= 0.611 (14%) ω_3= 1e5 (13%)
	Node 37	13.3182	0.0004	ω_1= 0.374 (99%) ω_2= 158 (0.67%)
Slc5a1	MNA	447.4476	<0.0001	ω_1= 0.0776 (90%) ω_2=100000 (10%)
	TSA	16.1794	0.0001	ω_1= 1e9 (100%)

B. Detailed exploratory aBSREL results (continued)

Gene	Branch	LRT	p-value	ω distribution
Slc2a2	ACA	30.9776	<0.0001	ω_1= 1.00 (37%) ω_2= 334 (63%)
	MHA	64.2921	<0.0001	ω_1= 1.00 (20%) ω_2= 1e5 (80%)
	Node 13	35.4885	<0.0001	ω_1= 0.00 (33%) ω_2= 1e5 (67%)
	MMY	19.7098	<0.0001	ω_1= 0.794 (12%) ω_2= 80.6 (88%)
Slc2a4	n/a	n/a	n/a	n/a
Slc2a5	EFU	28.7577	<0.0001	ω_1= 0.243 (11%) ω_2= 13.9 (89%)
	MSE	15.5125	0.0001	ω_1= 0.351 (93%) ω_2= 1e5 (6.7%)
	Node 39	12.1544	0.0008	ω_1= 0.024 (3.7%) ω_2= 13.2 (96%)
Treh	Node 11	22.4132	<0.0001	ω_1= 3.77 (100%)
	EFU	0.0221	0.0014	ω_1= 0.00 (78%) ω_2= 13.2 (22%)

B. Detailed exploratory aBSREL results (continued)

Gene	Branch	LRT	p-value	ω distribution
SI	MNA	96.3819	<0.0001	ω_1= 1.00 (98%) ω_2= 1.00 (1.8%) ω_3= 1e5 (0.60%)
	MSC	53.7631	<0.0001	ω_1= 0.301 (99%) ω_2= 6250 (0.5%)
	MWA	27.5404	<0.0001	ω_1= 0.00 (2.9%) ω_2= 1e5 (97%)
	Node 34	45.6658	<0.0001	ω_1= 1.00 (6.3%) ω_2= 9090 (94%)
	Node 39	38.1848	<0.0001	ω_1= 0.215 (97%) ω_2= 40.7 (3.1%)
	PHA	49.2379	<0.0001	ω_1= 1.00 (3.9%) ω_2= 3850 (96%)
	MSE	20.0862	<0.0001	ω_1= 0.200 (5%) ω_2= 1e5 (95%)
	Node 10	17.5613	0.0001	ω_1= 0.00 (92%) ω_2= 7.81 (8%)

A) aBSREL (adaptive Branch-Site Random Effects Likelihood) tests whether a proportion of sites have evolved under positive selection along each branch in the phylogeny. Baseline model refers to MG94xREV baseline model that infers a single omega rate per branch. Full adaptive model infers an optimized number of omega rate categories per branch. After aBSREL fits the full adaptive model, the Likelihood Ratio Test (LRT) is performed at each branch and compares the full model to a null model where branches are not allowed to have rate classes of ω>1. B) Detailed aBSREL results in bats. The results are from exploratory analysis where all branches are tested for positive selection. In this scenario, p-values at each branch must be corrected for multiple testing (using the Holm-Bonferroni correction). The Likelihood Ratio Test (LRT) is performed at each branch and compares the full model to a null model where branches are not allowed to have rate classes of ω>1. Branches and nodes under selection correspond to Fig. 2d.

https://doi.org/10.1038/s41559-024-02485-7

Extended Data Table 4 | Average blood glucose and gene expression changes

Species	ID	Blood glucose (mg/dL) (t=0)	Blood glucose (mg/dL) (t=10)	AVG Blood glucose change ± SE (mg/dL)	AVG Log2 fold change *Slc5a1*	AVG Log2 fold change *Slc2a2*	AVG Log2 fold change *Slc2a5*
Carollia perspicillata	**TT22- 57**	75	NA	440.6 ± 66.72	1.05*	0.468*	1.11**
	TT22-45	60	538				
	TT22-60	70	NA				
	TT22-59	83	343				
	TT22-83	54	719				
	TT22-01	78	342				
	TT22-03	70	606				
Glossophaga soricina	**TT22- 47**	91	NA	659.2 ± 29.27	1.26**	0.109	1.277**
	TT22-51	28	NA				
	TT22-50	63	750				
	TT22-52	59	707				
	TT22-53	29	750				
	TT22-54	67	597				
	TT22-62	40	750				
Pteronotus parnellii	**TT22-19**	57	NA	148.2 ± 48.82	1.813**	1.062*	2.605**
	TT22-28	41	NA				
	TT22-21	95	211				
	TT22-27	61	293				
	TT22-20	59	241				
	TT22-26	46	136				
	TT22-29	64	185				
Anoura geoffroyi	**TT22-38**	61	750	639.4 ± 20.96	0.331	-0.123*	1.719
	TT22-31	75	742				
	TT22-37	70	NA				
	TT22-30	66	NA				
	TT22-40	68	750				
	TT22-34	65	638				
	TT22-33	51	586				
Phyllostomus discolor	**TT23-34**	102	750	500.2 ± 107.54	NA	NA	NA
	TT22-64	121	750				
	TT23-55	52	497				
	TT23-46	73	750				
	TT22-101	96	198				
Artibeus jamaicensis	**TT22-68**	69	243	483 ± 96.38	0.006	0.350*	0.294*
	TT22-63	37	NA				
	TT22-81	91	750				
	TT22-86	29	632				
	TT22-80	41	328				
	TT22-66	58	750				
Micronycteris minuta	**TT22-15**	60	412	174.7 ± 94.57	NA	NA	NA
	TT22-72	83	112				
	TT22-48	149	292				

Change in blood glucose levels and change in gene expression 10-minutes after eating a 20% glucose solution. The fold change in gene expression was calculated from the mean log2 expression as follows: (μt=10/μt=0)-1. Each bat was fed a single dose of glucose (5.4 mg/kg body weight) after fasting (t=0). Samples in bold were used for HCR FISH (Extended Data Fig. 4), while others were sampled non-lethally. The change in gene expression were calculated from the following values found in Extended Data Fig. 4: *Carollia perspicillata* average log2 gene expression for *Slc5a1* μt=0=3.62 and μt=10=7.40; *Slc2a2* μt=0=5.24 and μt=10=7.69; *Slc2a5* μt=0=3.31 and μt=10=6.98. *Glossophaga soricina* average log2 gene expression for *Slc5a1* μt=0=3.06 and μt=10=6.91; *Slc2a2* μt=0=11.65 and μt=10=12.93; *Slc2a5* μt=0=2.73 and μt=10=6.22. *Pteronotus parnellii* average log2 gene expression for *Slc5a1* μt=0=2.61 and μt=10=7.35; *Slc2a2* μt=0=4.15 and μt=10=8.58; *Slc2a5* μt=0=1.95 and μt=10=7.03. *Anoura geoffroyi* average log2 gene expression for *Slc5a1* μt=0=4.63 and μt=10=4.55; *Slc2a2* μt=0=8.76 and μt=10=7.64; *Slc2a5* μt=0=1.85 and μt=10=5.02. *Phyllostomus discolor* average log2 gene expression for *Slc5a1* μt=10=5.75; *Slc2a2* μt=10=8.14; *Slc2a5* μt=10=no signal. *Artibeus jamaicensis* average log2 gene expression for *Slc5a1* μt=0=5.58 and μt=10=6.12; *Slc2a2* μt=0=5.13 and μt=10=6.93; *Slc2a5* μt=0=5.32 and μt=10=6.99. *Micronycteris minuta* average log2 gene expression for *Slc5a1* μt=60=3.84; *Slc2a2* μt=60=5.94; *Slc2a5* μt=60=no signal. Games-Howell pairwise comparisons with holm-bonferroni p-adjustments were performed using the ggstatsplot function in R. *pholm-adj<0.001; **pholm-adj<1e-6.

https://doi.org/10.1038/s41559-024-02485-7

Extended Data Table 5 | qPCR in triplicate

A. Heatmap ΔCt data

Species	ID	*Slc2a2* ΔCt (t = 0)	*Slc2a2* ΔCt (t = 10)	*Sglt1* ΔCt (t = 0)	*Sglt1* ΔCt (t = 10)	*Sl* ΔCt (t = 0)	*Sl* ΔCt (t = 10)
Pteronotus parnellii	TT18	6.86745521	NA	3.55971761	NA	5.844606344	NA
	TT19	10.2716057	NA	3.60320141	NA	4.35705189	NA
	TT23-07	7.70001793	NA	4.88196737	NA	5.262255404	NA
	TT21	NA	1.445631402	NA	1.4456314	NA	6.722156573
	TT23-08	NA	8.002572921	NA	6.66295049	NA	1.190077681
	TT27	NA	6.662950493	NA	8.00257292	NA	5.042138021
Anoura geoffroyi	TT37	3.85286167	NA	8.62575928	NA	-3.39176223	NA
	TT39	6.58676559	NA	6.71852256	NA	-1.34540214	NA
	TT23-60	7.70803494	NA	8.44735422	NA	-2.49798697	NA
	TT31	NA	8.401505792	NA	6.75625776	NA	0.327758008
	TT36	NA	5.6145058	NA	6.71947148	NA	-2.2649403
	TT38	NA	8.7758343	NA	9.3002665	NA	-1.4028583
	TT23-59	NA	5.584466769	NA	9.92668047	NA	-1.99588773
Artibeus jamaicensis	TT23-26	12.2918081	NA	15.6315313	NA	-1.40868706	NA
	TT23-28	NA	11.75367605	NA	14.1567788	NA	0.976657957
	TT69	NA	11.26822646	NA	14.1146598	NA	-1.62410615
Glossophaga soricina	TT23-20	-2.83783505	NA	7.97594834	NA	-2.54023774	NA
	TT50	NA	-3.03525001	NA	7.6965458	NA	-3.4618445
	TT52	NA	-3.07186737	NA	6.92463943	NA	-3.56332487
	TT23-22	NA	-1.99495814	NA	7.9596565	NA	-1.51345548
Carollia perspicillata	TT57	10.5452956	NA	5.55189654	NA	-2.08255449	NA
	TT60	11.4732742	NA	5.60353003	NA	-2.95612763	NA
	TT23-30	10.5643749	NA	6.87706993	NA	-1.1246682	NA
	TT59	NA	11.39375879	NA	6.17470782	NA	-2.1128141
	TT23-03	NA	11.40683157	NA	7.14829408	NA	-1.86943508

B. Violin Plot mean ΔΔCt data

Species	ID	*Slc2a2* ΔΔCt (t = 10)	*Sglt1* ΔΔCt (t = 10)	*Sl* ΔΔCt (t = 10)
Pteronotus parnellii	TT21	-6.83406155	2.349068866	1.567518694
	TT23-08	-1.61674245	-2.55946778	-3.9645602
	TT27	-0.27712003	0.436678094	-0.11249986
Anoura geoffroyi	TT31	2.352285059	-1.17428759	2.739475121
	TT36	-0.43471493	-1.21107388	0.146776813
	TT38	2.726613567	1.369721147	1.008858813
	TT23-59	-0.46475396	1.996135121	0.415829387
Artibeus jamaicensis	TT23-28	-1.02358161	-1.51687155	-0.21541909
	TT69	-0.53813203	-1.47475252	2.385345012
Glossophaga soricina	TT50	-0.19741496	-0.27940254	-0.92160676
	TT52	-0.23403232	-1.05130891	-1.02308713
	TT23-22	0.842876912	-0.01629184	1.02678226
Carollia perspicillata	TT59	0.532777238	0.163875653	-0.058364
	TT23-03	0.545850018	1.137461918	0.18501503

(A) RT-qPCR samples ran in triplicate against each target gene. Resulting Ct values from QuantStudio 7 Pro Real-time qPCR platform were averaged and ΔCt values were generated from the change between each target gene compared to GAPDH and visualized using heatmap (Extended Data 7). (B) Within each species tested, t=10 ΔCt values were compared against each t=0 ΔCt value. Taken as a grouped averages, as in this array, ΔΔCt of gene expression changes between the species were compared and visualized using violin plot (Extended Data 7).

nature portfolio

Corresponding author(s): Jasmin Camacho, Oscar E. MurilloGarcía, Nicolas Rohner

Last updated by author(s): May 27, 2024

Reporting Summary

Nature Portfolio wishes to improve the reproducibility of the work that we publish. This form provides structure for consistency and transparency in reporting. For further information on Nature Portfolio policies, see our Editorial Policies and the Editorial Policy Checklist.

Statistics

For all statistical analyses, confirm that the following items are present in the figure legend, table legend, main text, or Methods section.

n/a	Confirmed	
☐	☒	The exact sample size (*n*) for each experimental group/condition, given as a discrete number and unit of measurement
☐	☒	A statement on whether measurements were taken from distinct samples or whether the same sample was measured repeatedly
☐	☒	The statistical test(s) used AND whether they are one- or two-sided *Only common tests should be described solely by name; describe more complex techniques in the Methods section.*
☒	☐	A description of all covariates tested
☐	☒	A description of any assumptions or corrections, such as tests of normality and adjustment for multiple comparisons
☐	☒	A full description of the statistical parameters including central tendency (e.g. means) or other basic estimates (e.g. regression coefficient) AND variation (e.g. standard deviation) or associated estimates of uncertainty (e.g. confidence intervals)
☐	☒	For null hypothesis testing, the test statistic (e.g. *F*, *t*, *r*) with confidence intervals, effect sizes, degrees of freedom and *P* value noted *Give P values as exact values whenever suitable.*
☒	☐	For Bayesian analysis, information on the choice of priors and Markov chain Monte Carlo settings
☒	☐	For hierarchical and complex designs, identification of the appropriate level for tests and full reporting of outcomes
☒	☐	Estimates of effect sizes (e.g. Cohen's *d*, Pearson's *r*), indicating how they were calculated

Our web collection on statistics for biologists contains articles on many of the points above.

Software and code

Policy information about availability of computer code

Data collection	MAKER (v3.01.03), SwissProt/Uniprot v2021_03, RepeatMasker (open-4.0.7 with DB version 20170127, SIMRbase , HyPhy 2.5.33, FIJI v2.9.0 (ImageJ)
Data analysis	RStudio (ggstatsplot, phytools, ape)

For manuscripts utilizing custom algorithms or software that are central to the research but not yet described in published literature, software must be made available to editors and reviewers. We strongly encourage code deposition in a community repository (e.g. GitHub). See the Nature Portfolio guidelines for submitting code & software for further information.

Data

Policy information about availability of data

All manuscripts must include a data availability statement. This statement should provide the following information, where applicable:

- Accession codes, unique identifiers, or web links for publicly available datasets
- A description of any restrictions on data availability
- For clinical datasets or third party data, please ensure that the statement adheres to our policy

Original data underlying this manuscript can be accessed from the Stowers Original Data Repository at http://www.stowers.org/research/publications/LIBPB-2406

Research involving human participants, their data, or biological material

Policy information about studies with human participants or human data. See also policy information about sex, gender (identity/presentation), and sexual orientation and race, ethnicity and racism.

Reporting on sex and gender	*Use the terms sex (biological attribute) and gender (shaped by social and cultural circumstances) carefully in order to avoid confusing both terms. Indicate if findings apply to only one sex or gender; describe whether sex and gender were considered in study design; whether sex and/or gender was determined based on self-reporting or assigned and methods used. Provide in the source data disaggregated sex and gender data, where this information has been collected, and if consent has been obtained for sharing of individual-level data; provide overall numbers in this Reporting Summary. Please state if this information has not been collected. Report sex- and gender-based analyses where performed, justify reasons for lack of sex- and gender-based analysis.*
Reporting on race, ethnicity, or other socially relevant groupings	*Please specify the socially constructed or socially relevant categorization variable(s) used in your manuscript and explain why they were used. Please note that such variables should not be used as proxies for other socially constructed/relevant variables (for example, race or ethnicity should not be used as a proxy for socioeconomic status). Provide clear definitions of the relevant terms used, how they were provided (by the participants/respondents, the researchers, or third parties), and the method(s) used to classify people into the different categories (e.g. self-report, census or administrative data, social media data, etc.) Please provide details about how you controlled for confounding variables in your analyses.*
Population characteristics	*Describe the covariate-relevant population characteristics of the human research participants (e.g. age, genotypic information, past and current diagnosis and treatment categories). If you filled out the behavioural & social sciences study design questions and have nothing to add here, write "See above."*
Recruitment	*Describe how participants were recruited. Outline any potential self-selection bias or other biases that may be present and how these are likely to impact results.*
Ethics oversight	*Identify the organization(s) that approved the study protocol.*

Note that full information on the approval of the study protocol must also be provided in the manuscript.

Field-specific reporting

Please select the one below that is the best fit for your research. If you are not sure, read the appropriate sections before making your selection.

☐ Life sciences ☐ Behavioural & social sciences ☒ Ecological, evolutionary & environmental sciences

For a reference copy of the document with all sections, see nature.com/documents/nr-reporting-summary-flat.pdf

Ecological, evolutionary & environmental sciences study design

All studies must disclose on these points even when the disclosure is negative.

Study description	This study documents the sugar assimilation of ingested glucose, sucrose, and trehalose in multiple bat species.
Research sample	From field studies of wild bats, each individual bat was taxonomically identified, and their weight, age, sex, reproductive status and diet type was recorded. Juvenile individuals and pregnant or lactating females were excluded from the study due to high energy requirements and significant physiological changes during these stages, compared to non-pregnant or non-lactating adult individuals.
Sampling strategy	We opportunistically sampled bat species from mist netting. We tried to include at least three individuals per species per treatment. For morphology of the small intestine, we extracted the GI tract from individuals preserved in 70% ethanol from species found in museum collections. Additional GI tract samples were preserved in 4% paraformaldehyde from fasted and fed bats from common and abundant species for gene expression analysis.
Data collection	The blood glucose level was measured and recorded using a GlucoQuick G30a glucometer (Diabetrics®) with a range of 20-600 mg/dL and with an AlphaTRAK 2.0 glucometere (Zoetis) with a range of 20-750mg/dl. We measured the length of the duodenum through imaging the unfolded-stretched intestine of each species with a Canon EOS Rebel E7i. we compared relative intestine length as the gut length divided by torso length (shoulders to rump length). We used this measure to control by body size due to our focus on the intestine and where it is located, without adding measures related to the length of the rostrum or the tail, which can vary across bat species. Histological, TEM, and HCR fluorescence measurements were obtained with FIJI (ImageJ).
Timing and spatial scale	To determine blood glucose levels, a drop of blood was drawn from the forearm with a 30G lancet before the sugar bolus and 10, 30, and 60 minutes post-feeding. The bats individually remained in cloth bags between readings.
Data exclusions	The entire length of the duodenum was sectioned, but only sections with good morphology were used for data analysis. We want to avoid introducing artifacts from suboptimal tissue sections (missing cells, missing signal, folded tissue, etc).
Reproducibility	We sampled all healthy individuals we had access to by mist netting. A minimum of two individuals per species were used for each

Reproducibility	experiment type (blood measurements, museum samples, and gene expression). For genome comparisons, only one individual per species was available.
Randomization	Species were grouped by dietary preferences. The diet of the species was classified into trophic categories according to their food preference and morphological adaptations for the consumption of the food resource. We matched museum specimens to the localities of our field study (Colombia and Trinidad).
Blinding	Blinding was not possible as the co-first authors were familiar with the different species and their diets. The species differences were found throughout each level of data acquisition.

Did the study involve field work? ☒ Yes ☐ No

Field work, collection and transport

Field conditions	We opened mist nets between 18:00 and 24:00 h.
Location	Bats were captured between June 2019 and December 2020 in 11 localities of the dry tropical forest ecosystem in the department of Valle del Cauca, Colombia, some within the Dry Tropical Project from the Institute for Research and Preservation of the Cultural and Natural Heritage of Valle del Cauca (INCIVA). Bats were also captured in April 2022 in the dry tropical forest in Trinidad, West Indies.
Access & import/export	The fieldwork was made under the permit of the National Authority of Environmental Licenses and the Ministry of Environment and Sustainable Development of Colombia (Resolution 1070, August 28th, 2015) and under the permit of the Wildlife Section, Forestry Division, Ministry of Agriculture, Land and Marine Resources of the Republic of Trinidad and Tobago.
Disturbance	In some instances, bats were manually captured in their refuge.

Reporting for specific materials, systems and methods

We require information from authors about some types of materials, experimental systems and methods used in many studies. Here, indicate whether each material, system or method listed is relevant to your study. If you are not sure if a list item applies to your research, read the appropriate section before selecting a response.

Materials & experimental systems

n/a	Involved in the study
☒	☐ Antibodies
☒	☐ Eukaryotic cell lines
☒	☐ Palaeontology and archaeology
☐	☒ Animals and other organisms
☒	☐ Clinical data
☒	☐ Dual use research of concern
☒	☐ Plants

Methods

n/a	Involved in the study
☒	☐ ChIP-seq
☒	☐ Flow cytometry
☒	☐ MRI-based neuroimaging

Animals and other research organisms

Policy information about studies involving animals; ARRIVE guidelines recommended for reporting animal research, and Sex and Gender in Research

Laboratory animals	We did not use lab animals.
Wild animals	Bats were captured by mist nets. Here we include non-lethal GTT data for individuals with preference for fruit diet (n=79), mixed diet (n=55), nectar diet (n=18), insect diet (n=15), blood diet (n=14), and meat diet (n=1). For terminal time-points, all individuals were assigned a unique ID for museum deposit.
Reporting on sex	We did not encounter enough individuals per species to examine sex differences between males and females. Only adult males were compared for gene expression analysis.
Field-collected samples	Tissue samples from field collected species were stored at 4C in fixative and serially dehydrated to 100% methanol and stored at -20C in the lab until they were processed for histology and HCR experiments.
Ethics oversight	Ethical considerations for field studies were discussed and approved by the Stowers Institute IACUC protocol 2021-121.

Note that full information on the approval of the study protocol must also be provided in the manuscript.

Plants

Seed stocks

Report on the source of all seed stocks or other plant material used. If applicable, state the seed stock centre and catalogue number. If plant specimens were collected from the field, describe the collection location, date and sampling procedures.

Novel plant genotypes

Describe the methods by which all novel plant genotypes were produced. This includes those generated by transgenic approaches, gene editing, chemical/radiation-based mutagenesis and hybridization. For transgenic lines, describe the transformation method, the number of independent lines analyzed and the generation upon which experiments were performed. For gene-edited lines, describe the editor used, the endogenous sequence targeted for editing, the targeting guide RNA sequence (if applicable) and how the editor was applied.

Authentication

Describe any authentication procedures for each seed stock used or novel genotype generated. Describe any experiments used to assess the effect of a mutation and, where applicable, how potential secondary effects (e.g. second site T-DNA insertions, mosiacism, off-target gene editing) were examined.